Variable Ni isotope fractionation between Fe-oxyhydroxides and implications for the use of Ni isotopes as geochemical tracers

Bleuenn Guéguen, Jeffry Sorensen, Stefan Lalonde, Jasquelin Peña, Brandy Toner, Olivier J. Rouxel

Chemical Geology
March 2018, Volume 481 Pages 38-52
http://dx.doi.org/10.1016/j.chemgeo.2018.01.023
http://archimer.ifremer.fr/doc/00423/53473/

Variable Ni isotope fractionation between Fe-oxyhydroxides and implications for the use of Ni isotopes as geochemical tracers

Gueguen Bleuenn [1, 2, *], Sorensen Jeffry V. [3], Lalonde Stefan [1], Pena Jasquelin [4], Toner Brandy M. [3], Rouxel Olivier [2]

[1] Univ Brest, Lab Geosci Ocean, Inst Univ Europeen Mer, UMR 6538, F-29280 Plouzane, France.
[2] IFREMER, Ctr Brest, Unite Geosci Marines, F-29280 Plouzane, France.
[3] Univ Minnesota, Dept Soil Water & Climate, St Paul, MN 55108 USA.
[4] Univ Lausanne, Inst Earth Surface Dynam, CH-1015 Lausanne, Switzerland.

* Corresponding author : Bleuenn Gueguen, email address : bleuenn.gueguen@univ-brest.fr

Abstract :

Nickel (Ni) isotopes have recently emerged as a new biogeochemical tracer in marine environments, but our understanding of the mechanisms of Ni isotope fractionation in natural systems with regards to its fractionation by mineral surfaces is incomplete. This study aims to provide experimental constraints on Ni isotope fractionation during adsorption to goethite and 2-line ferrihydrite, two Fe minerals that vary in terms of distinct crystalline properties. We conducted two types of adsorption experiments: one with variable pH (5.0 to 8.0) and constant initial Ni concentration, one at a constant pH of 7.7 and variable initial Ni concentrations. Isotopic measurements were made on both the solid phase and the supernatant solutions in order to determine the Ni isotope fractionation factors ($\Delta 60/58Nimin\text{-}aq = \delta 60/58Nimin - \delta 60/58Niaq$) between the mineral and aqueous phases. Our results show preferential adsorption of lighter Ni isotopes during adsorption of Ni to Fe oxyhydroxides presumably under conditions of near equilibrium conditions. Adsorption to goethite generates the greatest fractionation, with $\Delta 60/58Nimin\text{-}aq = -0.77 \pm 0.23‰$ ($n = 14$, 2sd), whereas adsorption to 2-line ferrihydrite samples yield $\Delta 60/58Nimin\text{-}aq = -0.35 \pm 0.08‰$ ($n = 16$, 2sd). Using Ni K-edge extended X-ray absorption fine structure (EXAFS) spectroscopy, we found that Ni forms an inner-sphere complex and that its coordination environment does not vary significantly with pH nor with surface loading. In addition, we found no evidence of Ni incorporation into the mineral. We suggest that the more than two-fold increase in Ni isotope fractionation in goethite relative to 2-line ferrihydrite is due to the lower Ni-Fe coordination number in the second shell, which results in the formation of a weaker surface complex and thus favors the adsorption of lighter Ni isotopes. These results show that Ni isotope fractionation during sorption by Fe-oxyhydroxides is dependent on mineralogy, which has important implications for the use of Ni isotopes as environmental tracers and the interpretation of their record in sedimentary rocks.

Keywords : Fe-oxyhydroxides, Sorption experiments, Nickel isotopes

1. Introduction

Nickel is a micro-nutrient in modern oceans and displays a nutrient-type profile in seawater, where it is depleted in surface waters due to biological uptake (Bruland, 1980; Price and Morel, 1991; Morel and Price, 2003). The evolution of marine biogeochemical Ni cycling has become a topic of much interest as ancient metalliferous deposits because Banded Iron Formations (BIF) appear to record a dramatic decrease in marine Ni concentrations through geological time (Konhauser et al., 2009; Konhauser et al., 2015), attributed to a shift from ultramafic volcanism and eruption of Ni-rich komatiites to basaltic volcanism as the Earth's crust cooled. Iron-rich sedimentary rocks such as Granular Iron Formations (GIF) and BIF were deposited from seawater throughout much of the Precambrian and have been widely used as an archive to reconstruct the geochemical composition of seawater in Precambrian marine environments, in which Fe-oxyhydroxides were the carriers of trace metals (e.g., Bekker et al., 2010). Hence, Ni isotope systematics of Iron Formations hold great promise for the study of ancient biogeochemical cycles and paleo-environments. But first, the mechanisms of Ni isotope fractionation during Fe-oxyhydroxide precipitation and burial need to be well constrained.

The geochemical cycling of Ni in modern oceans is largely controlled by input from continental weathering and riverine transport and removal from seawater through precipitation in authigenic Mn-rich sediments (Sclater et al., 1976; Gall et al., 2013; Cameron and Vance, 2014). Preliminary investigations have shown that seawater is characterized by an average $\delta^{60/58}$Ni value of 1.44 ±0.15‰ (2sd, n=29) relative to the NIST SRM 986 international standard, which is heavier than the average crustal value (estimated at 0.05 ±0.05‰; Gueguen et al., 2013). The riverine input flux is estimated at a $\delta^{60/58}$Ni value of

0.80‰ with a range of values from 0.29 ‰ to 1.34‰ (Cameron and Vance, 2014). The oceanic output flux, dominated by authigenic Mn-oxyhydroxides (Krishnaswami, 1976; Leinen, 1987; Koschinsky and Halbach, 1995; Manceau et al., 2002; Peacock and Sherman, 2007b), has a $\delta^{60/58}$Ni value of ~1.7‰ (i.e., the average Ni isotope composition of hydrogenetic ferromanganese crusts as reported by Gall et al. (2013) and Gueguen et al. (2016)). The isotopically heavy signature of rivers relative to the bulk crust implies that a light Ni isotopic reservoir should be retained in the continental crust, probably during soil formation (Ratié et al., 2015). Based on isotopic mass balance considerations, Cameron and Vance (2014) identified a missing source of isotopically heavy Ni in modern oceans. Alternatively, the heavy Ni isotopic composition of seawater could be balanced by an oceanic sink enriched in light Ni isotopes, perhaps in sulfides (Gueguen et al., 2013; Hofmann et al., 2014) associated with anoxic or suboxic marine sediments enriched in organic matter that accumulate in reducing environments (e.g., continental margins with strong upwelling regimes, restricted anoxic basins, fjords). However, the role of organic-rich sediments in the Ni isotope mass balance is unclear as bulk $\delta^{60/58}$Ni of organic-rich sediments display a large range from 0.28‰ to 2.5‰ (Porter et al., 2014).

Large terrestrial Ni reservoirs exist in ultramafic complexes (Manceau and Calas, 1985; Valeton et al., 1987; Butt and Cluzel, 2013), and weathering of these complexes can lead to significant Ni enrichment in laterites. While Ni released during weathering of ultramafic complexes will have a greater affinity for Mn-oxides (Manceau et al., 1987), a significant portion of Ni is in fact sequestered in the abundant Fe-oxides (mostly goethite) formed during lateritization (Manceau et al., 2000; Quantin et al., 2008; Dublet et al., 2012; Dublet et al., 2014; Ratié et al., 2015). In a recent study, Ratié et al. (2015) demonstrated that weathering of ultramafic complexes leads to the enrichment of light Ni isotopes (by -0.47 ‰) in Ni-rich laterites relative to unweathered bedrock, consistent with the preferential loss of

heavy Ni isotopes to the mobile phase and eventually to the riverine flux. Nickel in these laterites is either incorporated into the mineral lattice or sorbed onto the mineral surface. Nickel sorption on Fe-oxyhydroxides may therefore influence the isotope signature of Ni in weathering environments, and in turn, the riverine flux of Ni to the oceans.

The use of Ni isotopes as biosignatures has also garnered attention in the recent literature and the evolution of Ni biogeochemical cycling in the ancient oceans may be recorded in the Ni isotope composition of coeval authigenic sediments. However, understanding the isotope fractionation of metals such as Ni during adsorption to Fe-oxides and other authigenic minerals is paramount to accurately reconstruct the biogeochemical cycling of nutrients using the sedimentary record. Wasylenki et al. (2015) reported the equilibrium Ni isotope fractionation factor during Ni sorption to ferrihydrite (experiments done at room temperature), showing an enrichment of the light Ni isotopes on the solid phase by -0.35 ±0.10 ‰ (1 sd). However, further studies are needed in order to evaluate in more detail the mechanisms and range of parameters controlling Ni isotope fractionation during adsorption onto mineral phases, including the effects of coordination environment or the type of mineral phase (e.g., poorly crystalline versus more crystalline phases). For instance, different Ni isotope fractionation could be expected among different Fe-oxyhydroxides based on coordination chemistry considerations, because this effect has been observed for other metal/metalloid isotope systems such as Cu, Ge, Mo and Zn (Pokrovsky et al., 2008; Li and Liu, 2010; Wasylenki et al., 2011; Pokrovsky et al., 2014). These experimental data are crucial to interpret the trace metal isotopic records in Iron Formations, where the mechanism of formation of Fe-oxyhydroxides- precursor mineral phases and scavenging of trace metals are poorly known, and to evaluate the preservation of the isotopic signal during recrystallization. The role of iron oxides recrystallization on the Ni cycling is also important

to consider as it could have impacted the Ni signal preserved in Iron Formations (Frierdich et al., 2011).

To address this problem, we conducted Ni adsorption experiments on two synthetic Fe-oxyhydroxides, 2-line ferrihydrite and goethite, as a function of pH, variable Ni loading to pre-formed minerals, (i.e., no co-precipitation) and duration of experiments. Our goal is to mechanistically understand the isotope fractionation during Ni adsorption to Fe-phases with different crystallinity, with special consideration to Ni speciation, coordination, and structure of adsorbent. The local coordination environment of Ni at the mineral surface was evaluated by Ni K-edge EXAFS spectroscopy, while the isotopic fractionation of Ni between solid and aqueous phases were measured by Multi Collector-Inductively Coupled Plasma-Mass Spectrometer (MC-ICP-MS) using double-spike (^{61}Ni-^{62}Ni) correction of instrumental mass bias. Our results build on the results of Wasylenki et al. (2015) regarding the causes for Ni isotope fractionation. We expand on the role of Fe-oxides in the transfer of continental Ni to the oceans and in the biogeochemical cycling of Ni isotopes, furthering the development of Ni isotopes as a geochemical tracer in surface environments.

2. Materials and methods

We used synthetic mineral phases to investigate surface driven Ni isotope fractionation. The use of synthetic mineral phases allowed for Ni K-edge EXAFS spectroscopy on samples with low Ni concentration without interference from significant amounts of incorporated Ni. Goethite (α-FeOOH) and 2-line ferrihydrite were synthesized by raising the pH of a $Fe(NO_3)_3$ solution with KOH at 25°C. Goethite was formed by heating the solid precipitate at 70°C for 60 hours following the protocol of Cornell and Schwertmann (2003). The precipitates were washed three times with ultrapure water and centrifuged at

7,000 rpm for 30 minutes. The goethite was stored freeze-dried while the 2-line ferrihydrite was synthesized within 48 hours of each experiment and stored at -30°C. The synthetic minerals were characterized by BET (Brunauer-Emmett-Teller) surface area, powder X-ray diffraction, and electrophoretic mobility. For BET, samples were dried and degassed at 150°C before specific surface area was measured by N_2 adsorption (Micromeritics Tristar II 3020). The specific surface areas for goethite and 2-line ferrihydrite were 25.5 and 119 ± 3 m^2/g, respectively. Bulk powder X-ray diffraction was performed using a Pananalytical X'Pert Pro diffractometer (Characterization Facility, University of Minnesota). Mineral surface charge, which is reflected in surface electrokinetic potential, was determined using a ZetaPALS analyzer (Brookhaven Instruments Corp.) for 0.98 - 1.44 g/L of mineral suspended in ultrapure water. Instrumental settings consisted of an applied voltage of 7.54V and electric field of 9.29 V/cm. Data were acquired over 3 cycles of 5 measurements per mineral (Electronic Annex, Table A1).

2.1. Nickel sorption experiments

For the Ni sorption experiments, a stock solution of 17 mmol/L Ni (1000 mg/L Ni) was made with a $Ni(NO_3)_2 \cdot H_2O(aq)$ salt (Fischer Scientific). Aqueous suspensions were prepared with 0.15 g of goethite or 2-line ferrihydrite in 150 mL of 0.05 mol/L $NaNO_3$ in 250 mL Teflon bottles. The Fe-oxyhydroxides were allowed to equilibrate for 24 hours at the target experimental pH before the addition of an aliquot of Ni from the stock solution. Nickel was added slowly using a micropipette over a 15 minutes' period, with continuous mixing with a Teflon-coated stir bar to reduce changes to the pH of the suspension. A control consisting of the mineral in 0.05 mol/L $NaNO_3$ solution with no Ni added was included with each set of experiments and Ni in the blank did not exceed 0.1% of the total amount of Ni

150 measured during Ni sorption experiments. Samples were named according to the adsorbent
151 (i.e., “Fh” for 2-line ferrihydrite and “Goe” for goethite) and the type of experiment (i.e.,
152 “pH” for pH-dependent experiments, “C” for varying initial Ni concentration experiments and
153 “T” for time-dependent experiments).

154 Nickel sorption experiments (Table 1) were performed as a function of pH (pH 5.0,
155 6.0, 7.0, 7.7 and 8.0) with an initial Ni concentration of 170 µmol/L Ni (10 mg/L Ni). A
156 separate set of Ni sorption experiments were also performed at pH 7.7 as a function of initial
157 Ni concentration (17, 85, 170, 341, and 426 µmol/L Ni). The suspension pH was maintained
158 constant within ± 0.2 pH units with a custom-built pH control system consisting of 6 Hanna
159 Instruments HI 504 controllers, each equipped with a Thermo Scientific Orion 9110 pH
160 electrode. Adjustments of the pH were made with additions of 0.05 mol/L HCl and 0.05
161 mol/L NaOH using two 3-way General Valve™ solenoid valves and a Manostat Carter
162 peristaltic cassette pump. The pH electrodes were calibrated using pH 4 and pH 7 commercial
163 buffers before each experiment. After the addition of Ni, the suspension was allowed to react
164 for 24 hours before the solution was separated from the solids by vacuum filtration (0.22 µm
165 polycarbonate filter, Millipore). The solids were not rinsed prior to storage or analysis. After
166 filtration, the supernatant solution was refrigerated at 2°C until analysis by ICP-MS and the
167 solid material on filter was stored at -20° C. The solid-phase samples on the filter membranes
168 were cut in half and reserved for Ni K-edge EXAFS spectroscopy and isotopic analysis.

169 Time-dependent experiments were done to check whether kinetic isotopic effects are
170 affecting our experiments (Table 2). They were performed at a fixed pH of 7.7 and at two
171 different initial Ni concentrations of 170 µmol/L and 426 µmol/L, in order to assess the
172 potential effect of dissolved Ni concentration (i.e., Ni loading) on Ni isotope fractionation
173 factor. Four different batches were prepared for each initial Ni concentration and were
174 allowed to react for 18 (or 19 hours for 2-line ferrihydrite), 20, 22, and 23 hours, respectively.

A maximum equilibration time of 24 hours was chosen based on our initial test time-dependent experiments with goethite and ferrihydrite in which the aqueous Ni concentration stabilized after 18 to 23 hours of reaction, consistent with experimental design implemented by Wasylenki et al. (2015). These findings are consistent with bulk chemical equilibrium and were used to choose the reaction time for the adsorption experiments. This also prevents the potential effect of diffusion-controlled penetration of Ni into Fe (oxy)hydroxides on Ni isotope fractionation, since this process has been shown to occur over long (week to month) timescales, while surface adsorption reaches completion within a few hours (Bruemmer et al., 1988). As discussed below, at bulk chemical equilibrium the mineral continues to exchange Ni with the aqueous phase, so isotopic changes are still possible. By contrast, no net change in loading to the mineral occurs, implying that the Ni concentration in the mineral is constant.

2.2. Nickel K-edge EXAFS spectroscopy

Nickel K-edge EXAFS spectroscopy measurements were conducted at the Advanced Photon Source (Argonne National Laboratory) at beamline 20-BM in fluorescence mode using a 12-element Canberra germanium detector. The Ni-sorbed minerals were prepared for Ni K-edge EXAFS analysis by thawing to room temperature and transferring from the filter to a mylar adhesive with a microspatula. Multiple mylar layers were stacked (6-8 layers) and the edges sealed to form an envelope around the sample. Measurements were conducted at room temperature and individual scans were examined for systematic changes in peak-position or shape to detect photon-induced sample alteration; none was observed. Multiple scans were averaged to improve the signal to noise ratio. The Athena program was used for averaging replicate scans and energy calibration (Ni foil with inflection point set to 8334.5 eV), and the Artemis program was used to generate phase and amplitude paths for Ni K-edge EXAFS

fitting (Ravel and Newville, 2005). Data reduction, including background subtraction and conversion to k-space, and shell-by-shell fitting were performed using the SixPack software package (Webb, 2005) with the following settings: E_0=8347 eV, R*bkg* =1.0 Å (Kelly et al., 2008), a Gaussian pre-edge function, quadratic post-edge function, no clamping, default spline knots value, a Kaiser-Bessel window function, and a *k*-weight =3. The amplitude reduction factor, S_0^2 = 0.96, was determined by fitting the first coordination shell of aqueous published standards ($NiCl_2$ and Ni-EDTA) (Peña et al., 2010). Fits were evaluated using the calculated R-factor with a value of 0.05 or less representing a reasonable fit (Kelly et al., 2008).

X-ray absorption spectra were collected from 8130 to 9300 eV. Models for the adsorption geometry of Ni were based on the assumption that Ni coordinates to Fe octahedra via edge-sharing or corner-sharing linkages. First, the Ni-O shell was fit with all parameters varied. The optimized parameters for the first shell were constrained in subsequent fits, which included second-shell Ni-Fe paths.

The Ni-Fe second shell was modeled assuming to the occurrence of short and long bond distances, following the model used for Ni/Zn sorption on ferrihydrite (Arai, 2008; Cismasu et al., 2013). Specifically, two types of bond orientations between Fe and Ni octahedral were modeled. Type 1 is comprised of a Ni octahedron that shares an edge, two bond via two shared oxygen molecules, with an Fe octahedra (mineral surface). Type 2 is comprised of a Ni octahedron that shares a corner, or one bond via a shared oxygen, with an Fe octahedra (mineral surface). Type 1 bond distances are shorter and share more bonds with the mineral surface than Type 2. Distortion of the Ni-O coordination sphere can be influenced by either the number of bonds with the mineral surface, or geometric strain introduced due to the type of surface site (e.g., number/type of Fe octahedra) to which the Ni binds.

The Ni K-edge EXAFS model was based on published coordination number (CN) ratios of a short and long Ni-Fe and Zn-Fe paths in the second shell of Ni K-edge EXAFS data from Ni/Zn-adsorbed 2-line ferrihydrite samples (Table 3) (Manceau and Gates, 1997; Carvalho-E-Silva et al., 2003; Arai, 2008; Dublet et al., 2012; Cismasu et al., 2013). Reported CN ratios for Ni-sorbed 2-line ferrihydrite ranged from 0.4 :0.7 (CN_{short} :CN_{long}) with a maximum total second-shell CN of 5 (Arai, 2008). Thus, CN_{short} :CN_{long} ratios of 1:1 to 4:5 were tested in the model. A ratio of 2:3 best described the Ni K-edge EXAFS data in both fit statistics and uncertainty of varied parameters. In the final model, two type 1 Ni-Fe paths were modeled for every three type 2 Ni-Fe paths. The uncertainties on the CN values are between 0.144 and 0.931 (estimated to be ~25% of the CN value) and the uncertainties on the interatomic distances are between 0.0078 and 0.0618 Å.

2.3. Aqueous speciation of Ni

The aqueous speciation of Ni was calculated for the initial experimental conditions using the MINEQL+ v.4.6 software program (Environmental Research Softaware) with default stability constants. The calculations used the initial Ni concentrations (17, 85, 170, 341, and 426 µmol Ni/L), pH range (5.0 to 8.0 in 20 steps), ionic strength (0.05 mol/L $NaNO_3$), and partial pressure of CO_2 g (0.03943 vol%) for a system in contact with the atmosphere and showed that no Ni precipitation is predicted for our experimental conditions. We used Ni surface complexation values for bidentate adsorption on goethite [2 =SOH + Ni^{2+} $\Leftrightarrow$=2(SOH)Ni + $2H^+$, log K = -2.45] from Xu et al. (2006), and for ferrihydrite, monodentate adsorption per Dzombak and Morel (1990) (their classic two-site ferrihydrite model, strong and weak sites, as already included in vMINTEQ). For aqueous speciation calculations during adsorption modeling, the default vMINTEQ thermo.vdb database was used, which is an

expanded version of the MINTEQA2 database. Between pH 5.0 and 7.0, the dominant Ni species in aqueous solution, under the initial experimental conditions considered here, is the Ni^{2+} (hexaquo) (> 88 %). In addition to Ni^{2+} (hexaquo), $NiNO_3^+$ is present and accounts for > 11% of the Ni in solution. For the experiments with a pH value greater than 7.0, the aqueous Ni species include minor contributions from $NiHCO_3^+$ and $NiCO_3^0$. Slow addition of Ni during the experiments over a 15-minutes period reduced the risk of precipitation of Ni above pH 7.8. For the experiments at pH 7.7, Ni occurs as: (1) 83.7% Ni^{2+} (hexaquo); (2) 10.7 % $NiNO_3^+$; (3) 4.1 % $NiHCO_3^+$; and (4) 1.5 % $NiCO_3^0$ for initial Ni concentrations ranging from 17 to 426 µmol/L.

2.4. Concentration determinations and column chromatographic purification of Ni

All manipulations were performed in a class 1000 clean room and exclusively used acid-cleaned plasticware and teflonware. Solid samples were digested in 6 mol/L HCl at room temperature for 72 hours. The total concentrations of Ni and Fe in the solids were determined by quadrupole ICP-MS (X-series2, Thermo Scientific) at the Pôle Spectrométrie Océan (PSO, Brest, France). Nickel concentrations in the filtrates were first estimated by mass balance using the initial concentrations in solutions used at the start of each experiment and the Ni concentrations in the solids determined by quadrupole ICP-MS at the end of the experiment. Nickel concentrations were then recalculated by isotope dilution after isotope measurements.

For the separation of Ni onto chromatographic columns, an aliquot of each filtrate was evaporated to dryness at 80°C prior to redissolution in 1 ml of 6 mol/L HCl. A full description of the purification method can be found in Gueguen et al. (2013). Briefly, our two-step separation procedure involved: (1) separation of Fe onto an anion exchange chromatographic resin (BioRad AG1-X8, 100-200 mesh); (2) separation of Ni from the remaining matrix using

a Ni-specific resin (Ni-Spec by Eichrom). This Ni-resin contains dimethylglyoxime (DMG) functional groups, which complexes Ni in ammonium citrate solutions at pH 8-9. Nickel is then eluted with 3 mol/L HNO_3 after breakdown of the Ni-DMG complex.

2.5. Ni isotope mass spectrometry and double-spike correction scheme

Nickel isotope compositions were measured by MC-ICP-MS (Neptune, Thermo Scientific) at the PSO (Brest, France) using a double spike for mass bias correction following the method described in Gueguen et al. (2013). The double spike is a mixture of ^{61}Ni and ^{62}Ni that was added to samples at spike/natural ratio of 1 prior to the chromatographic separation on Ni-specific resin. Corrected ratios were calculated using an iterative scheme following the method described by Siebert et al. (2001). An ESI (Elemental Scientific Inc., USA) desolvating introduction system (ApexQ) was employed for all measurements. The nine Faraday cups of the instrument allowed simultaneous measurement of Ni isotopes ^{58}Ni, ^{60}Ni, ^{61}Ni, ^{62}Ni, ^{64}Ni, and potential isobaric interferences from Zn (measured on ^{66}Zn) and Fe (measured on ^{57}Fe). Argon oxide interferences (e.g., $^{40}Ar^{18}O^{+}$ on $^{58}Ni^{+}$ and $^{40}Ar^{17}O$ on ^{57}Fe) were resolved using the medium resolution mode of the MC-ICP-MS.

Nickel isotope values were reported according to the conventional delta notation (equation 1) relative to the Ni international isotopic standard NIST SRM 986 :

$$\delta^{60/58}\text{Ni (‰)} = \left(^{60/58}\text{Ni}_{\text{sample}}/^{60/58}\text{Ni}_{\text{NIST986}} - 1\right) \times 1000 \qquad (1)$$

For each sample, 50 measurement cycles were performed, resulting in an internal standard error (2se) value typically between 0.02 and 0.04 ‰. The external precision was evaluated through the duplicated measurements of geostandards (USGS Nod-P-1, $\delta^{60/58}$Ni=0.33‰; and USGS Nod-A-1, $\delta^{60/58}$Ni=1.04‰) and was found to be ~0.06 ‰ (2sd).

3. Results

3.1. Nickel sorption by Fe oxyhydroxides

The loadings of Ni onto both 2-line ferrihydrite and goethite expressed in terms of the percent of Ni sorbed for pH-dependent and varying initial [Ni] experiments are displayed in Table 1. The sorption of Ni onto 2-line ferrihydrite for pH ranging from 5.0 to 8.0 (i.e., pH-dependent experiments, with initial Ni concentration of 170 µmol/L) resulted in Ni uptake between < 1% and 45% translating into 0.02 to 0.62 µmol Ni/m^2 mineral (Figure 1a). At pH 7.7 (varying initial Ni concentrations experiments, 17 to 426 µmol/L Ni), final Ni loadings on 2-line ferrihydrite ranged from 0.11 to 1.71 µmol Ni/m^2 mineral (Figure 1), which correspond to a percentage of sorbed Ni between 25% and 78%.

Nickel sorption to goethite at pH 5.0, 6.0, and 8.0 resulted in Ni uptake between < 1% and 4.3% of the initial 170 µmol/L aqueous Ni (Figure 1), corresponding to Ni loadings ranging from 0.04 and 0.28 µmol Ni/m^2. At pH 7.7, Ni uptake from solutions with initial concentrations of 17, 170, and 426 µmol/L Ni yielded final Ni loadings onto the mineral between 0.63 to 1.33 µmol Ni/m^2, corresponding to percentage of sorbed Ni between 8% and 19%.

Zeta potential measurements at pH 7 indicated that 2-line ferrihydrite exhibits a net negative surface charge with a value of -3.44 mV (Electronic Annex, Table A1). Zeta potential measurements at pH 7 indicated that goethite exhibits a net positive surface charge with a value of +3.46 mV. 2-line ferrihydrite has more Ni-sorbed at pH 7 than goethite, which is consistent with the more negative surface charge of 2-line ferrihydrite relative to goethite.

3.2. Surface complexation modeling

Constant capacitance surface complexation modeling (CCM) for Ni adsorption to 2-line ferrihydrite and goethite (Figure 2) was implemented using adsorption parameters provided by Dzombak and Morel (1990), Xu et al. (2006) and Davis and Kent (1990), in order to verify that sorption processes control Ni behavior in our experiments. Our experimental data for 2-line ferrihydrite were in good agreement with the surface complexation model calculated with parameters from Dzombak and Morel (1990) (Figure 2). The best fit of our data for Ni adsorption to goethite was obtained with a constant capacitance model (Figure 2) generated using adsorption constants from Xu et al. (2006) for bidentate adsorption in the Ni-goethite system, our BET-measured surface area of 25.5 m^2/g, solid concentrations close to 1 g/L, and a goethite site density of 1 site per nm^2. Adopting higher literature values for the latter (e.g., 2.3 sites per nm^2 (Davis and Kent, 1990) or 6 sites per nm^2 (Xu et al., 2006)) results in model adsorption values significantly higher than what was observed. Finally, it is important to point out that the CCM is a simple surface complexation model that integrates a smaller number of parameters in comparison to the diffuse-layer model and the triple-layer models (Hayes et al., 1991) and thus may not approximate natural conditions as closely.

3.3. Nickel K-edge EXAFS Spectroscopy

Nickel K-edge EXAFS spectra were collected for six Ni-sorbed 2-line ferrihydrite samples (Fh-pH-05, Fh-C-07, Fh-C-08, Fh-C-09, and Fh-C-10) and one Ni-sorbed goethite sample (Goe-C-06) as indicated in Table 1. The Ni K-edge EXAFS spectra collected for the 2-line ferrihydrite samples at pH 7.7 and 8.0 are similar in phase and amplitude despite different Ni-loadings and pH values (displayed in k-space with best fits; Figure 3). All Ni K-edge EXAFS spectra were fit with ~ 6 Ni-O atom pairs in the first-shell at a distance of 2.05 ±

0.01 Å (Table 3). For the Ni-Fe second-shell atom pairs, two sub-shells were required to describe the data: ~ 1.5 Ni-Fe (type 1) at 3.10 ± 0.02 Å and ~ 0.6 Ni-Fe (type 2) at 3.56-3.60 ± 0.06 Å. Errors in the second shell coordination numbers were estimated using the fractional parameter error as an indicator. As these error values were low we estimated CN error to be ~25% of the value.

The magnitude and imaginary portion of the Fourier transformed Ni K-edge EXAFS spectra and fits are displayed in Figure 4. The only notable difference in the Ni K-edge EXAFS derived fit parameters obtained for 2-line ferrihydrite and goethite was a lower Ni-Fe coordination number in the type 1 second shell for Ni-sorbed goethite. Nickel sorbed to goethite had on average 1.0 ± 0.4 Fe in its second shell, while Ni-sorbed to 2-line ferrihydrite had an average of 2.2 ± 0.56 Fe atoms in its second shell (Table 3). This difference can be viewed by comparing peak amplitudes of the two minerals whereby 2-line ferrihydrite samples have greater peak amplitudes than goethite. The Ni K-edge EXAFS data are also consistent with the formation of inner-sphere complexes with no evidence for a separate Ni phase.

3.4. The Ni isotope composition of sorbed Ni and supernatant solutions

The Ni isotope composition of the initial Ni stock solution was determined at $\delta^{60/58}$Ni = -0.33 ± 0.05 ‰ (2sd, n=4, Table 1). The Ni isotope compositions of mineral-associated Ni (i.e, sorbed onto 2-line ferrihydrite and goethite) and solution are reported in Table 1.

The difference in Ni isotopic composition between the mineral sorbed-Ni and Ni remaining in solution, which we define as the fractionation factor, is expressed as $\Delta^{60/58}Ni_{min\text{-}aq}$ (equation 2) according to:

$$\Delta^{60/58}Ni_{min\text{-}aq} = \delta^{60/58}Ni_{mineral} - \delta^{60/58}Ni_{aqueous} \quad (2)$$

Figure 5 presents $\delta^{60/58}$Ni values of the mineral and the associated filtrate versus corresponding percent Ni sorbed in pH-dependent, variable initial Ni concentration and time-dependent experiments. The results show a systematic enrichment in light Ni isotope compared to the starting solution during Ni sorption to the mineral surface, which is accompanied by enrichment of the residual aqueous Ni in heavy isotopes. Isotopic mass balance (equation 3), was verified for each sample and was consistent within uncertainty with the Ni isotope composition of the original stock solution (Table 1).

$$\delta^{60/58}Ni_{bulk} = (\%Ni_{sorbed}/100 \times \delta^{60/58}Ni_{mineral}) + ((1 - \%Ni_{sorbed}/100) \times \delta^{60/58}Ni_{aqueous}) \quad (3)$$

The magnitude of the Ni isotope fractionation factor $\Delta^{60/58}Ni_{min\text{-}aq}$ (equation 2) between the solid phase and aqueous phase is larger for goethite (-0.77 ±0.23 ‰) than for 2-line ferrihydrite (-0.32 ±0.20 ‰), with no significant correlation with the percentage of adsorption (Figures 5 and 7). We observe consistent and similar $\Delta^{60/58}Ni_{min\text{-}aq}$ values for pH-dependent and variable Ni concentration experiments for 2-line ferrihydrite on the one hand, and for goethite on the other hand.

The pH-dependent adsorption experiments on 2-line ferrihydrite yielded surface loadings from 0.02 to 0.62 µmol Ni/m^2 mineral with $\Delta^{60/58}Ni_{min\text{-}aq}$ values ranging from -0.37 to -0.03 ‰ (Figure 6). At low loadings of Ni onto 2-line ferrihydrite, i.e., 0.02 – 0.04 µmol Ni/m^2 mineral which correspond to 1 and 3% percent of to the total added Ni sorbed in the pH 5.0 and 6.0 experiments, Ni isotopes were not fractionated ($\Delta^{60/58}Ni_{min\text{-}aq}$ = -0.03‰) or weakly fractionated ($\Delta^{60/58}Ni_{min\text{-}aq}$ = -0.12 ‰) respectively. Although Figure 6 seems to indicate that decreasing $\Delta^{60/58}Ni_{min\text{-}aq}$ values are correlated with increasing pH for 2-line ferrihydrite, we

399 think these data are an artifact since low pH values (5.0 and 6.0) also correspond to very low
400 Ni loadings (see discussion). For this reason, we decided to not include these data when
401 discussing average Ni isotope fractionation factors. In contrast, at pH 7.7, the percent Ni
402 sorbed was generally higher and Ni loadings of 0.32 – 1.71 µmol Ni/m^2 mineral were
403 achieved, which represent between 23 and 78% Ni-sorbed on 2-line ferrihydrite. This gave a
404 range of $\Delta^{60/58}Ni_{min\text{-}aq}$ values between -0.40 and -0.24 ‰ (Figures 6 and 7).
405 Nickel sorption by goethite for the pH-dependent experiment was minimal, ranging
406 from 0.6 to 4% of the initial Ni (corresponding to loadings of 0.04 – 0.28 µmol Ni/m^2
407 mineral), and Ni isotope fractionation was characterized by $\Delta^{60/58}Ni_{min\text{-}aq}$ values between -0.96
408 and -0.70 ‰ (Figure 6). At pH 7.7 and for different initial Ni concentrations, final loadings of
409 Ni of 0.63 to 1.33 µmol Ni/m^2 mineral yielded $\Delta^{60/58}Ni_{\ min\text{-}aq}$ values between -1.03 and -0.78
410 ‰ (Figure 6). Goethite with the lowest loading of Ni (also corresponding to the lowest pH)
411 displayed the smallest Ni isotope fractionation factor relative to other samples, with
412 $\Delta^{60/58}Ni_{min\text{-}aq}$ = -0.70 ‰ and -0.88 ‰ for pH 5.0 and 6.0, respectively. The largest $\Delta^{60/58}Ni_{min\text{-}aq}$
413 value of -1.03 ‰ was measured at pH 7.7 for goethite with the highest Ni loading.
414 Time-dependent experiments were performed in order to identify potential kinetic
415 effects (i.e., non-equilibrium Ni fractionation) in our experiments. Experiments were
416 conducted for four different durations, i.e., 18 or 19, 20, 22, and 23 hours and for two
417 different initial Ni concentrations of 170 µmol/L and 426 µmol/L (Table 2). The Ni isotope
418 fractionation factor $\Delta^{60/58}Ni_{min\text{-}aq}$ is between -0.77 and -0.72 ‰ (average $\Delta^{60/58}Ni_{min\text{-}aq}$ = -0.75
419 ± 0.05 ‰; 2sd, n=4) and $\Delta^{60/58}Ni_{min\text{-}aq}$ values are between -0.73 to -0.62 ‰ (average
420 $\Delta^{60/58}Ni_{min\text{-}aq}$ = -0.67 ± 0.09 ‰; 2sd, n=4) for the two experiments respectively.
421
422 **4. Discussion**
423

Previous work on non-traditional isotope systems, such as Mo (Barling and Anbar, 2004; Goldberg et al., 2009; Kashiwabara et al., 2009; Wasylenki et al., 2011), Zn (Pokrovsky et al., 2005; Juillot et al., 2008), Cu (Balistrieri et al., 2008; Pokrovsky et al., 2008), Tl (Rehkämper et al., 2002), Cd (Wasylenki et al., 2014), Hg (Jiskra et al., 2012), Fe (Icopini et al., 2004; Mikutta et al., 2009; Beard et al., 2010; Wu et al., 2011; Wu et al., 2012; Frierdich et al., 2014), Ge (Li and Liu, 2010; Pokrovsky et al., 2014), and Se (Mitchell et al., 2013) have shown that adsorption reactions are often accompanied by significant isotope fractionation processes that may vary according to sorbent composition and sorbate structure. By contrast, sorption of Cr(VI) to Fe-oxyhydroxides is not accompanied by significant isotope fractionation (Ellis et al., 2004). Hence, the combination of spectroscopic and isotopic measurements is essential for understanding isotopic fractionation processes. Here, we discuss the result of both approaches to address the mechanisms and significance of Ni isotope fractionation during Ni sorption to Fe-oxyhydroxides.

4.1. Surface coordination of Ni at the mineral surface

Coordination chemistry (i.e., coordination number, bond length) correlates with the extent of isotope fractionation because shorter bond lengths (i.e., stiffer bonds) or lower coordination numbers favor enrichment of heavier isotopes (e.g., Schauble, 2004; Pokrovsky et al., 2005). The first coordination shell of a metal is comprised of oxygen atoms. Variations of the coordination number of the metal (e.g., between the aqueous phase and the solid phase) during adsorption of a transition metal to the surface of any given Fe-oxyhydroxide mineral is a common cause for isotope fractionation. For instance, heavy isotope enrichment during Zn sorption on ferrihydrite was accounted for by a decrease in the coordination number of the aqueous species relative to the adsorbed species. According to EXAFS data, the adsorption of

449 Zn onto ferrihydrite produces a significant shift in Zn coordination number, from 6 in the
450 solution to 4 in the solid, while Zn sorbed on goethite occurs in octahedral coordination, i.e.,
451 similar to aqueous Zn. The larger isotope fractionation factor measured for ferrihydrite
452 relative to goethite can thus be explained by a different coordination environment of the
453 sorbed Zn (i.e., 4 for ferrihydrite and 6 for goethite) and differences in Zn-O bond stiffness
454 (i.e., 1.96 Å for ferrihydrite and 2.11 Å for goethite; Juillot et al., 2008). For Ni, isotopic
455 fractionation cannot be related to changes in the coordination number between aqueous Ni
456 and sorbed Ni because Ni exclusively occurs in coordination 6 in the natural environment.
457 The length of Ni – O bonds in water is 2.1 Å compared to the 2.05 Å observed when Ni is
458 sorbed to the mineral surface (Soper et al., 1977), therefore, heavier Ni isotopes enrichment
459 should be expected during sorption to the mineral surface. The systematic enrichment in
460 lighter Ni isotopes on the mineral phase found in this study and in Wasylenki et al. (2015)
461 precludes this option.

462 Wasylenki et al. (2015) suggest that distortion of the coordination environment after
463 Ni sorption to ferrihydrite could explain light Ni isotopes enrichment of the mineral surface.
464 Given our Ni K-edge EXAFS data quality it was not possible to support or refute this
465 hypothesis because we could not achieve fitting multiple Ni-O paths to the Ni-O shell (first
466 coordination shell). However, the number of bonds between Ni and surface oxygens, which is
467 reflected in the second shell parameters (i.e., surface complex geometry), may cause slight
468 distortion or distribution of the electron density in the first coordination shell, even if they
469 cannot be captured by the Ni K-edge EXAFS data. Thus, we argue that the number of bonds
470 between Ni and surface oxygens could distort the first coordination shell.

471 Consistent with previous studies (Manceau et al., 2000; Carvalho-E-Silva et al., 2003;
472 Arai, 2008; Dublet et al., 2012) adsorbed Ni displayed octahedral coordination (Electronic
473 Annex, Table A2). For an inner-sphere surface complex of Ni on Fe oxyhydroxides, the

second major coordination shell is composed of Fe atoms. The interatomic distances between Ni and Fe, as measured by Ni K-edge EXAFS spectroscopy, define the local coordination environment of the Ni surface species and Ni sorbed on ferrihydrite and goethite have been studied in detail (Waychunas et al., 2002; Arai, 2008; Juillot et al., 2008; Dublet et al., 2012; Cismasu et al., 2013). It was demonstrated that Ni sorbed on ferrihydrite occurs in octahedral coordination between Ni-O_6 and Fe-O_6 polyhedra with interatomic distances in the range of 3.05-3.08 Å for edge-sharing type 1 surface complexes, 3.19-3.12 Å for edge-sharing type 2, and 4.03-4.07 Å for corner-sharing (Arai, 2008). Type 1 edge sharing is between Ni and Fe octahedra in the chains and type 2 surface complexes is between Ni and Fe octahedra in the rows (Arai, 2008). The interatomic distances modeled here for goethite samples reflect the three Fe-Fe second-shell interatomic distances for edge-sharing coordination between Ni and a chain of Fe-O_6 octahedra (i.e., type 1), edge-sharing between chains of Fe-O_6 octahedra (i.e., type 2), and corner-sharing Fe-O_6 octahedra between double chains (Manceau and Drits, 1993).

Incorporation of Ni into Fe-oxyhydroxides lattices is possible, but our Ni K-edge EXAFS data shows the absence of Ni incorporation in the minerals. Cornell et al. (1992) reported Ni incorporation into synthetic goethite at ~5% of the total molar fraction and several studies showed that incorporation of Ni in goethite occurs via diffusion into the mineral lattice where Ni can occupy vacant Fe positions in synthetic goethite (Barrow et al., 2012; Brümmer et al., 2013). Fischer et al. (2007) showed that Ni reaction with the goethite surface is continuous with time and that Ni is incorporated via diffusion in the lattice structure of the mineral. Wasylenki et al. (2015) reported nearly identical isotopic signatures for surface sorbed Ni and incorporated Ni, suggesting that the influence of incorporated Ni is negligible in the isotopic budget and that potential Ni isotope fractionation during diffusion can be precluded.

499 The best Ni K-edge EXAFS model for Ni sorbed to 2-line ferrihydrite data, with two
500 Ni-Fe distances in the second shell, is consistent with a short Ni-Fe distance produced by
501 edge-sharing polyhedra (3.10 ± 0.02 Å) in addition to a longer Ni-Fe distance produced by a
502 combination of edge-sharing and corner-sharing polyhedra not resolved by our Ni K-edge
503 EXAFS data (3.57 ± 0.06 Å). The data quality for the Ni-sorbed goethite prevented a robust
504 second-shell fit to the Ni K-edge EXAFS. However, the fit results were consistent with a Ni-
505 Fe atom pair at 3.07 ± 0.03 Å and revealed a difference relative between goethite and 2-line
506 ferrihydrite in the Ni-Fe coordination number. The Ni K-edge EXAFS measurements on
507 goethite and 2-line ferrihydrite from this study also indicate that the Ni coordination
508 environment was similar among all samples. Therefore, the difference in Ni isotope
509 fractionation between the two minerals may be due to minor differences in surface site density
510 and distribution. Since no detectable difference in surface speciation was observed as a
511 function of Ni loading to the 2-line ferrihydrite surface at pH 7.7 or as a function of pH (7.7
512 versus 8.0), alternative variable parameters such as protonation state of the mineral, surface
513 complex geometry (e.g., number of bonds between Ni and mineral surface), surface coverage
514 or bond lengths between the two minerals might have influenced Ni isotope fractionation.
515
516 *4.2. Nickel isotope fractionation factors during Ni adsorption to Fe-oxyhydroxides*
517
518 In the case of equilibrium isotopic fractionation, the fractionation factor between
519 mineral and solution, the $\alpha_{min\text{-}aq}$ value (related to $\Delta^{60/58}Ni_{min\text{-}aq}$ values as $\approx 10^3.\ln \alpha_{min\text{-}aq}$),
520 ultimately depends on the difference in bond stiffness between two species involved in the
521 reaction. In a closed system, the Ni isotope composition of the solution and mineral-bound Ni
522 are related to the proportion of Ni sorption to the mineral (Figure 5). If equilibrium isotope
523 fractionation is maintained during the experiment, the fractionation factor, $\Delta^{60/58}Ni_{min\text{-}aq}$,

should remain constant regardless of the percentage of Ni adsorption and duration of the experiments. We recognize that equilibrium isotope fractionation is best demonstrated using the 3-isotopes method (Wu et al., 2011), which allows the determination of the rate of isotopic exchange and extrapolate the isotope fractionation factors during incomplete isotope exchange. Here, we mainly relied on the constant Ni isotope fractionation factor between solution and mineral during the reaction progress in order to derive equilibrium $\Delta^{60/58}Ni_{min\text{-}aq}$ values. Results obtained for 2-line ferrihydrite and goethite (i.e., pH dependent, concentration dependent, and time dependent) are for the most part consistent with isotopic equilibrium in a closed system (i.e., constant $\Delta^{60/58}Ni_{min\text{-}aq}$ values), although significant departure from this relationship is observed at low percentage of Ni sorption (Figure 7) and in one goethite sample (i.e., the variable initial Ni concentrations experiments with 19.3% Ni-sorbed (Figure 5)).

In order to derive meaningful Ni isotope fractionation factors from the experimental data, the % of Ni adsorption should be generally comprised between 5% to 95%, i.e., too low or too high values may pose problem in the determination of $\delta^{60/58}Ni$ of the mineral and solution, respectively. Using this more restricted dataset, we determine an average $\Delta^{60/58}Ni_{min\text{-}aq}$ = -0.32 ±0.20 ‰ for the 2-line ferrihydrite and $\Delta^{60/58}Ni_{min\text{-}aq}$ = -0.77 ±0.23 ‰ for goethite.

For time-dependent experiments, we determine a range of $\Delta^{60/58}Ni_{min\text{-}aq}$ values for the 2-line ferrihydrite between -0.32 ±0.04 and -0.38 ±0.06‰, and for goethite between -0.65 ±0.07 and -0.77 ±0.07‰. Therefore, $\Delta^{60/58}Ni_{min\text{-}aq}$ values do not vary within uncertainties over the course of the experiments. This is in agreement with previous results of Wasylenki et al. (2015) showing no variations in $\Delta^{60/58}Ni_{min\text{-}aq}$ values for 2-line ferrihydrite for experiment duration between a few hours to 30 days. There is also no appreciable difference in the magnitude of Ni isotope fractionation factor depending on the initial Ni concentration and sorption %, i.e., $\Delta^{60/58}Ni_{min\text{-}aq}$ = -0.35 ±0.01 ‰ (2sd, n=4) for an initial Ni concentration of

549 170 µmol/L and $\Delta^{60/58}Ni_{min\text{-}aq}$ = -0.36 ±0.05 ‰ (2sd, n=4) for an initial Ni concentration of
550 426 µmol/L (Table 2). Average $\Delta^{60/58}Ni_{min\text{-}aq}$ values for 2-line ferrihydrite and goethite time-
551 dependent experiments are also similar to the average value calculated for the pH-dependent
552 and varying initial Ni concentrations experiments suggesting that our experiments are at
553 isotopic equilibrium. The duration of experiments is the same for low Ni-sorbed samples than
554 for high Ni-sorbed samples. Therefore, if there were any kinetic effects we would expect them
555 to be similar whatever the amount of sorbed Ni or that larger isotope fractionation would
556 occur for low Ni-sorbed samples compared to high Ni-sorbed samples which is not the case in
557 our experiments. Although these experiments did not allow the determination of isotopic
558 exchange rates between the solution and the mineral, which would have required shorter
559 experiment duration, we suggest that isotopic equilibrium was likely achieved in our
560 experiments. This assumption is also consistent with previous goethite adsorption experiments
561 for Cu and Zn isotopes systematics (Pokrovsky et al., 2005; Pokrovsky et al., 2008) for which
562 isotope fractionation factors were similar for short duration experiments (~20 hours) than for
563 long duration experiments (~ 100 days).

564 The smaller Ni isotope fractionation factors for goethite and 2-line ferrihydrite at low
565 % (Figure 7) can be explained in several ways: (1) non-equilibrium fractionation (i.e., kinetic
566 fractionation processes) due to partially irreversible reaction between sorbed Ni on the
567 mineral and Ni in solution; (2) a change in coordination chemistry in the mineral with pH
568 and/or Ni loading; and (3) retention of aqueous Ni on the mineral during filtration, leading to
569 incomplete separation of Ni in mineral and Ni in solution. As explained above, time-
570 dependent experiments suggest that isotopic equilibrium is achieved which, thus, discounts
571 hypothesis (1). Hypothesis (2) can also be ruled out since no change in coordination
572 chemistry as a function of pH was observed in the Ni K-edge EXAFS measurements. We
573 propose that the low $\Delta^{60/58}Ni_{min\text{-}aq}$ values measured in samples prepared at low pH may be due

574 to the presence of a small fraction of the supernatant solution that remained trapped in the
575 mineral even after filtering, which would mute Ni isotope fractionation during adsorption.
576 Using the final Ni concentration measured in supernatant solutions and the estimated volume
577 of water present in the mineral, we calculated that the supernatant solution should contribute
578 between 0.0002 and 0.0070 µmol Ni/m^2 for 2-line ferrihydrite. Hence, for low Ni-loading in
579 the 2-line ferrihydrite experiments, Ni in solution may account for between 13 % and 44 % of
580 the total Ni in the sorbed fraction. This mixing effect is the most plausible explanation
581 (hypothesis 3) for the variation in $\Delta^{60/58}Ni_{min\text{-}aq}$ values (i.e., decrease) at low Ni-loading.
582
583 *4.3. Differences in Ni isotope fractionation between goethite and 2-line ferrihydrite*
584
585 Our experiments showed that Ni sorbed to goethite is twice more fractionated towards
586 lighter $\Delta^{60/58}Ni_{min\text{-}aq}$ values (~ -0.77 ‰) than Ni sorbed to 2-line ferrihydrite (~ -0.35 ‰).
587 Nickel species in solution that are likely to be adsorbed onto minerals are the Ni^{2+}
588 (hexaquo) species (Peacock and Sherman, 2007a). The surface complexation model reported
589 in Figure 2 predicts that under the experimental conditions used in our study Ni should sorb to
590 goethite to a greater extent than we observed in our experiments. At pH values less than ~ 8.0,
591 the expected point of zero net charge for goethite is such that it should be positively charged.
592 In contrast, the zeta potential measurements for 2-line ferrihydrite indicate a net negatively
593 charged surface. The net negative surface charge of 2-line ferrihydrite tends to attract
594 dissolved cations to its surface while the net positive surface charge of goethite tends to repel
595 dissolved cations and ferrihydrite has a higher surface area than goethite. This is in agreement
596 with the strong uptake of Ni from solution by 2-line ferrihydrite observed in our experiments
597 and predicted by our surface complexation model (Figure 2).

598 Two different modes of isotope fractionation are then possible during Ni adsorption to
599 Fe-oxyhydroxides. One involves isotopic exchange among aqueous species in solution
600 followed by preferential adsorption of one of these species onto the mineral phase. This
601 mechanism may lead to contrasting isotope composition between the fluid and mineral, as
602 previously observed for the Mo isotope system (Siebert et al., 2003; Barling and Anbar,
603 2004). An alternative mechanism of fractionation may take place directly during metal
604 adsorption and involves the preferential adsorption of one isotope from the aqueous phase
605 onto the solid phase because of, for instance, differences in coordination chemistry or kinetic
606 effects. These two mechanisms are not mutually exclusive and combination of the two is
607 likely to occur in natural systems. Pokrovsky et al. (2014) identified five mechanisms that
608 could be responsible for equilibrium isotope fractionation during sorption reactions: (1)
609 protonation of metal species in solution or on the mineral surface; (2) mineral surface
610 coverage and distribution of weak sites versus strong sites; (3) bond distances between the
611 metal and oxygen atoms and the presence of other atoms in the mineral structure; (4) change
612 in coordination between the fluid and the solid phase; and (5) binding mode of the metal.
613 Below we evaluate each of these mechanisms in light of the results from our study.
614 Mechanism (1) : Protonation of aqueous or sorbed Ni. As a divalent cation, Ni has a
615 relatively low ionic potential, e.g., in contrast to Fe^{3+} and Al^{3+}. Hence, $Ni(H_2O)_6^{2+}$ does not
616 readily undergo hydrolysis and Ni tends to form relatively weak aqueous complexes with
617 ligands when compared to trivalent cations. In addition, because we expect the presence of a
618 single aqueous Ni species, $Ni(H_2O)_6^{2+}$, in our experiments there should be no isotopic
619 fractionation occurring in solution.
620 Mechanism (2) : Mineral surface coverage and distribution of weak and strong sites.
621 Villalobos et al. (2003) demonstrated that goethite synthesized with variable NaOH addition
622 rates yield variable site densities that are in turn reflected in adsorption behavior. The goethite

623 minerals synthesized in our study appear to fall on the low end of surface site concentrations
624 reported in literature for goethite. Our Ni K-edge EXAFS data and fits revealed no detectable
625 differences between low and high Ni loadings onto 2-line ferrihydrite. Therefore, we have no
626 evidence to support a fractionation mechanism based on discrimination between weak and
627 strong sorption sites. The Ni loading data when normalized to mineral surface area show no
628 distinct differences between 2-line ferrihydrite and goethite in terms of range or magnitude of
629 Ni surface coverage (Figure 1 and Table 1). This suggests that mineral surface loading does
630 not explain the Ni isotope fractionation observed in our experiments.

631 Mechanism (3) : Bond distances between the metal and oxygen atoms and the
632 presence of other atoms in the mineral structure. The minerals studied here were synthesized
633 in the laboratory and are free of impurities. In addition, as discussed above, the Ni-O first-
634 shell interatomic distances are indistinguishable among our 2-line ferrihydrite and goethite
635 sorbents.

636 Mechanism (4): Change in coordination between the fluid and the solid phase. Based
637 on thermodynamic modeling, we expect the aqueous Ni speciation is > 80% Ni^{2+} (hexaquo),
638 $Ni(H_2O)_6^{2+}$, and in octahedral coordination with O. Based on our Ni K-edge EXAFS data, the
639 Ni sorbed to 2-line ferrihydrite and goethite is also in octahedral coordination with O.

640 Mechanism (5): Metal bonding environment. The Ni K-edge EXAFS data and fit
641 results indicate that the local coordination environment for Ni at the mineral surface is similar
642 for all Ni loadings and pH values for 2-line ferrihydrite. To determine whether we can extend
643 this finding to goethite, we compared two samples for which Ni K-edge EXAFS data were
644 collected : (1) Goe-C-06 (1.33 µmol Ni/m^2) and Fh-C-10 (1.71 µmol Ni/m^2). These two
645 samples have similar Ni loadings when the amount of adsorbed Ni is normalized by specific
646 surface area (Table 1) and the Ni K-edge EXAFS-derived fit parameters for the Ni-O shell are
647 identical within errors. In other words, the Ni species have the same coordination number and

the same bond lengths for Ni-O (recall some of the coordinating oxygens are contributed by the mineral and waters of hydration). The only difference in Ni speciation between the two samples is a lower Ni-Fe coordination number in the second shell for Ni-sorbed goethite. On average, the Ni sorbed to goethite has only 1.0 Fe (range 0.6-1.5) in its second shell, while Ni-sorbed to 2-line ferrihydrite has 2.2 Fe (range 1.8-2.7) (Table 3). This difference in surface complex geometry, which may originate from the structure of goethite as discussed below, suggest that the number of bonds formed between Ni and surface oxygen atoms, as indicated by the number of Ni-Fe near neighbors, may influence the distribution of electron density in the first coordination shell of Ni and thus influence its isotopic fractionation.

Of these possible mechanisms, only mechanism (5) 'binding mode of the metal' provides a good explanation for our data. Specifically, we observe a subtle difference between the Ni-Fe second-shell coordination environment when comparing two Ni-sorbed mineral samples having similar Ni loading when expressed in terms of surface area rather than total mass. Nickel sorbed to goethite has fewer Fe atoms in the second-shell than Ni sorbed to 2-line ferrihydrite. The goethite structure is known to generate three different surface functional groups based on the number of Fe atoms bonded to a surface oxygen (Essington, 2003) : type (1) $\equiv Fe_3\text{-}O^{1/2-}$, type (2) $\equiv Fe_2\text{-}O^{1-}$, and type (3) $\equiv Fe\text{-}O^{3/2-}$. In our experiments, sorption of $Ni(H_2O)_6^{2+}$ by site type (3) is most consistent with the results. In addition, fewer Fe atoms in the second coordination shell is consistent with weaker surface complexes and the observed enrichment of light Ni isotopes in the Ni-sorbed to goethite sample leading to larger isotopic fractionation (i.e., larger fractionation factor $\Delta\delta^{60/58}Ni_{min\text{-}aq}$) than for 2-line ferrihydrite.

4.4. Implications for Ni isotope biogeochemical cycling in modern and ancient surface environments

673 *4.4.1. Nickel isotope systematics during continental weathering*

674

675 In modern Earth surface environments, Fe-oxyhydroxides are likely an important
676 carrier of Ni in riverine suspended sediments (Turekian, 1977; Snodgrass, 1980; Callender,
677 2014) and in soils (Dublet et al., 2012; Ratié et al., 2015). Snodgrass (1980) showed that Ni
678 occurs in solution (0.5% only), as adsorbed species (3.1%), as precipitated inorganic phases or
679 particle coatings (47%), as organic matter-bound complexes (14.9%) and as crystalline
680 material (34.4%). Martin and Meybeck (1979) showed that Ni occurs mainly in the truly
681 dissolved phase. However, a proportion of the total dissolved pool consists of Ni sorbed to Fe
682 and Mn-oxides colloids and particles (Mouvet and Bourg, 1983; Gaillardet et al., 2014) while
683 a significant proportion of Ni is associated with colloidal organic matter and organic
684 compounds (Vasyukova et al., 2010). Considering that the proportion of each of these Ni
685 pools in rivers may vary depending on environmental and geological settings, Ni speciation
686 may exert a strong influence on the Ni isotope composition of rivers. Bedrock lithology, rock
687 alteration processes and soil formation may be also important. For example, the Ni isotope
688 composition of Ni-rich laterites forming through weathering of ultramafic complexes
689 indicates an enrichment in light Ni isotopes by -0.47 ‰ compared to the bedrock composition
690 (Ratié et al., 2015). Nickel isotope fractionation during adsorption to Fe-oxyhydroxides might
691 explain the observed light isotopes enrichment in weathering environment, and by isotopic
692 mass balance, the overall enrichment in heavy isotopes in rivers (Cameron and Vance, 2014).
693 This would indicate a significant role for Fe in Ni isotopic cycling on continental surfaces and
694 more specifically in the delivery of Ni to the oceans both in terms of elemental flux and
695 isotopic composition.

696 In natural environments, the reaction rate for the transformation of ferrihydrite to
697 goethite can be relatively rapid (< 500 days) and does not depend on pH (Schwertmann et al.,

2004), but ferrihydrite can be metastable in some environments (Navrotsky et al., 2008; Toner et al., 2012). The presence of large amounts of Ni incorporated in Fe-oxyhydroxides has been shown to slow the transformation of poorly crystalline Fe-oxyhydroxides to more crystalline phases (Cornell et al., 1992; Cornell and Schwertmann, 2003). During dissolution of Fe(III)-oxyhydroxides, Ni is released more slowly than Fe, which leads to enrichment in Ni in the residual solid phase (Cornell et al., 1992). The presence of organic ligands in seawater may also affect the crystallization of ferrihydrite and its transformation to goethite (Cornell and Schwertmann, 1979). Therefore, in the case of differential Ni isotope fractionation between the two mineral phases as observed in this study, the overall Ni isotope composition of Fe-oxyhydroxides may be controlled by the nature of the initial mineral phase precipitated.

Based on our results, we propose that Ni adsorption on Fe-oxyhydroxides is likely to be a major mechanism for explaining the enrichment in heavy Ni isotopes in river water compared to the Bulk Silicate Earth by ~ 0.6-0.7 ‰ (Cameron and Vance, 2014). However, one should also consider the possibility that the present-day main river discharges (e.g., Amazon river) may contain some anthropogenic Ni as a by-product of fossil fuel burning, which may alter both the natural concentration of Ni in rivers and its isotopic composition. For instance, Gueguen et al. (2013) report a $\delta^{60/58}$Ni value of 0.5 ‰ in coal, which is heavier than the Bulk Silicate Earth isotopic composition. Such anthropogenic input could also explain the apparent Ni isotopic imbalance in the ocean (Cameron and Vance, 2014), thereby implying that Ni delivery to the ocean occurs under non steady-state conditions.

4.4.2. Application to Precambrian seawater chemistry and ancient Ni biogeochemical cycling

The marine biogeochemical cycle of Ni experienced major perturbations during the Precambrian (Konhauser et al., 2009; Konhauser et al., 2015), including an apparent sharp

723 decrease in the Ni delivery to the ocean at the onset of the Great Oxidation Event, at ca. 2.5
724 Ga. Under the overall anoxic conditions and high Ni bioavailability of the Archean oceans,
725 microorganisms such as methanogens may have been important primary producers. Given
726 that methanogens fractionate light Ni isotopes by up to ~ -1.5 ‰ (Cameron et al., 2009), such
727 a shift in Ni utilization in the oceans should have left characteristic imprints in the Ni isotopic
728 composition of Precambrian seawater. Because Fe-oxyhydroxides were probably an important
729 host phase for Ni in ancient marine environments (Konhauser et al., 2009), an understanding
730 of Ni isotope fractionation during sorption to ferrihydrite or goethite is critical for inferring
731 the Ni isotopic composition of Precambrian seawater from the Precambrian sediment record
732 (Wasylenki et al., 2015). Tracing the evolution of Ni isotopic composition in Precambrian
733 seawater by investigating BIFs could provide meaningful insights into the coevolution of the
734 chemical composition of seawater with biological evolution and diversification (Bekker et al.,
735 2010). However, Fe-oxides such as hematite and magnetite are the predominant carrier of Ni
736 in these deposits, although accessory minerals such as silicates (e.g., stilpnomelane) and
737 carbonates may be also important. Because the nature and origin of the Fe-oxyhydroxide
738 precursor in BIF remain poorly known, interpretations based on the Ni isotope composition in
739 BIF should be made with significant caution given the range of possible fractionation factors
740 for different mineral types (e.g., ferrihydrite vs. goethite) and adsorption mechanisms.
741 Our results show that Ni isotope fractionation during abiotic reactions involving
742 adsorption on Fe-oxides are of the same order of magnitude as for biotic reactions (i.e.,
743 Cameron et al., 2009) and vary between different mineral surfaces i.e., from ~ -0.35 ‰ (2-line
744 ferrihydrite) to ~ -0.77 ‰ (goethite). Hence, the use of Ni isotopes as biosignatures should be
745 approached with caution, as Ni isotope fractionation produced by abiotic processes may mask
746 any isotope signals related to biotic processes. This issue is critical for BIF studies because
747 the large extent of Fe precipitation in seawater, leading to the accumulation of freshly formed

748 Fe-oxyhydroxides at the seafloor as likely BIF precursors, may also shift the isotopic
749 composition Ni remaining in seawater.
750 In a previous study, Wasylenki et al. (2015) suggested that Ni isotopes in BIF should
751 be offset by ~ -0.35 ‰ relatively to seawater. We further propose that such an offset is likely
752 a minimum value, considering that fractionation up to ~ -0.77 ‰ is observed during sorption
753 to goethite, regardless of potential kinetic isotope effects. Clearly, further study investigating
754 the preservation of Ni isotope signatures during Fe-oxyhydroxide recrystallization to hematite
755 and magnetite is warranted in order to directly apply Ni isotope systematics to the BIF record.
756 Although Wasylenki et al. (2015) showed that there was apparently no isotope fractionation
757 during aging of ferrihydrite and recrystallization to goethite and hematite, they did not
758 determine the proportion of ferrihydrite that has recrystallized, and longer experimental
759 durations as well as heating of the system should be explored to better evaluate the effect of
760 ferrihydrite aging on Ni isotopes. The effect of silica (Eickhoff et al., 2014) and the possibility
761 that it could affect the Ni isotope fractionation factor during BIF formation, has also to be
762 considered when investigating the BIF record.
763
764 **5. Summary**
765
766 Consistent with previous studies (Wasylenki et al., 2015), we found that Ni isotopes
767 are readily fractionated towards light Ni isotopes during adsorption to Fe-oxyhydroxide
768 minerals. Building on that work, we have demonstrated that Ni sorbed to 2-line ferrihydrite is
769 less fractionated than Ni sorbed to goethite with average $\Delta^{60/58}Ni_{min\text{-}aq}$ values of -0.35 ±0.08
770 ‰ and -0.77 ±0.23 ‰, respectively. No difference in $\Delta^{60/58}Ni_{min\text{-}aq}$ values was observed either
771 as a function of Ni loading or as a function of pH in both 2-line ferrihydrite and goethite. For
772 both 2-line ferrihydrite and goethite, Ni K-edge EXAFS results indicate that there are no

measurable changes in Ni coordination as a function of pH or final Ni loading to the mineral. In addition, on the timescale of our experiments there is no evidence that Ni is structurally incorporated into either mineral. The only difference we found between the two minerals is the lower Ni-Fe coordination number in the second shell of goethite, and we argue that this may account for a larger Ni isotope fractionation factor (~ -0.77 ‰) to goethite in comparison to 2-line ferrihydrite (~ -0.35 ‰). Although additional data are required to strengthen the conclusions on kinetic experiments, first results suggest that Ni concentrations and $\Delta^{60/58}Ni_{min\text{-}aq}$ values do not vary with time, as it would be expected for suspensions at equilibrium. In addition, the $\Delta^{60/58}Ni_{min\text{-}aq}$ values for 2-line ferrihydrite and goethite in the kinetic experiments on average are similar to the $\Delta^{60/58}Ni_{min\text{-}aq}$ values calculated for the pH-dependent and varying initial Ni concentrations experiments suggesting that our experiments are at isotopic equilibrium over a duration of ~24 hours.

The magnitude of isotope fractionation suggests that Ni adsorption to Fe-oxyhydroxides is a significant process controlling Ni isotope abundances in the natural environment. Our study also shows that such Ni isotope fractionation factors during Ni adsorption on Fe-oxides are in the same direction and extent as for biological uptake of Ni by methanogens. Hence, these findings provide important insights into the mechanisms of Ni isotope fractionation in natural environments, as well as cautionary guidelines for interpreting Ni isotope (bio)signatures in ancient sedimentary rocks. This study underpins the need to further investigate the influence of weathering and soil processes, as well as anthropogenic inputs, on the Ni isotopic composition of rivers and, in turn, on the mass balance of Ni isotopes in seawater.

Acknowledgements:

We thank Marie-Laure Rouget for technical assistance during ICP-MS-quadrupole data acquisition; Yoan Germain for technical assistance in the clean labs; Emmanuel Ponzevera for technical assistance during MC-ICP-MS measurements; Rick Knurr for ICP-MS analyses (Aqueous Geochemistry Lab, University of Minnesota); Dale Brewe, Steve Heald, and Mali Balasubramanian for assistance with Ni K-edge EXAFS data collection (20-BM, Advanced Photon Source, Argonne National Laboratory); Lindsey Briscoe for construction of the pH stat system; Lee Penn (Department of Chemistry, University of Minnesota) for access to the zeta potential instrumentation, Kyungsoo Yoo (Department of Soil, Water & Climate) for access to the BET instrumentation; and the Kuehnast Endowment Fund (Department of Soil, Water, and Climate, University of Minnesota) for research support for JVS. We further thank Yves Fouquet and Ewan Pelleter for fruitfull discussions. The powder X-ray diffraction was conducted at the Characterization Facility, University of Minnesota. The Ni K-edge EXAFS data collection was conducted at the Advanced Photon Source (APS), beamline 20-BM. The APS is an Office of Science User Facility operated by the U.S. Department of Energy (DOE) Office of Science by Argonne National Laboratory under contract number DE-AC02-06CH11357. Supports from ANR-10-LABX-19-01 LabexMER and Europole Mer are also acknowledged.

Figure captions:

Figure 1: Nickel loading to minerals (µmol/m^2 mineral) as a function of (a) pH (data from pH-dependent experiments) and (b) initial aqueous concentration of Ni (µmol/L) (data from varying initial Ni concentration experiments).

Figure 2: Surface complexation modeling (SCM) using a Constant Capacitance Model (CCM) and experimental data from this study showing percent of Ni sorbed versus solution pH for (a) 2-line ferrihydrite and (b) goethite. The SCM (bold line) fits the experimental data well (filled circles) for 2-line ferrihydrite (a) while experimental data (filled stars) for goethite deviates from the SCM (dashed line) (b). A possible explanation for this discrepancy was that very little Ni was adsorbed (< 5 %) on the goethite surface, contributing non-negligible uncertainty to the determination of percent Ni sorbed.

Figure 3: Summary of Ni K-edge EXAFS spectra in k-space for Ni-sorbed 2-line ferrihydrite at pH 7.7 and 8.0. Data are displayed as solid lines, while fits to data are displayed as dashed lines.

Figure 4: Summary of Fourier transformed data (magnitude and imaginary part) and fits for Ni-sorbed 2-line ferrihydrite at pH 7.7 and 8.0. Data are displayed as solid lines, while fits to data are displayed as dashed lines.

Figure 5: Nickel isotope composition (‰) of minerals (circles) and supernatant solutions (squares) for pH-dependent (pink symbols), variable initial Ni concentration in solution (brown symbols) and time-dependent experiments (blue symbols) for (a) 2-line ferrihydrite and (b) goethite. The straight black line in the two plots represents the Ni isotope composition of the starting Ni solution ($\delta^{60/58}$Ni = -0.33 ‰). The error bar (2sd) corresponds the reproducibility of the geostandards (~ ±0.06 ‰; see section 2.5 for explanation). Values are consistent between each experiment according to the type of mineral, i.e., -0.35 ±0.08 ‰ for 2-line ferrihydrite and -0.77 ±0.23 ‰ for goethite. The average $\delta^{60/58}$Ni value for 2-line ferrihydrite does not take into account the very low Ni-sorbed samples (unfilled datapoints on

the figure, see main text for explanation). Note also that the x-axis is different for 2-line ferrihydrite and goethite because the range of %-adsorption is lower for goethite than for 2-line ferrihydrite.

Figure 6: Ni isotope fractionation factors ($\Delta^{60/58}Ni_{min\text{-}aq} = \delta^{60/58}Ni_{mineral} - \delta^{60/58}Ni_{aqueous}$) versus (a) pH using results from pH-dependent experiments and (b) final Ni loading to the mineral (µmol/g mineral) for goethite (diamonds) and 2-line ferrihydrite (circles). The error bar (2se) corresponds to the value of ±0.05 ‰ as the highest value determined by error propagation on samples (see section 3.4 for more explanation). The unfilled datapoints in plot (a) correspond to very low Ni-sorbed to 2-line ferrihydrite (see main text for explanation).

Figure 7: Ni isotope fractionation factors ($\Delta^{60/58}Ni_{min\text{-}aq} = \delta^{60/58}Ni_{mineral} - \delta^{60/58}Ni_{aqueous}$) versus %-adsorption for (a) 2-line ferrihydrite and (b) goethite for each type of experiment. Pink dots are for pH-dependent experiments, brown dots for the variable initial Ni concentration experiments and blue dots are for the time-dependent experiments. The unfilled red datapoints in plot (a) (2-line ferrihydrite) correspond to very low Ni-sorbed samples (see main text for explanation).

Table captions:

Table 1: Sample information, summary of experimental conditions, Ni loading to the mineral and Ni isotope composition (‰) of mineral phases and supernatant solutions for pH-dependent experiments, variable Ni concentration experiments. Non-filled symbols correspond to the very low sorbed Ni samples (see text for discussion).

873 **Table 2:** Sample information, summary of experimental conditions, Ni loading to the mineral
874 and Ni isotope composition (‰) of mineral phases and supernatant solutions for time-
875 dependent experiments.
876
877 **Table 3**: Summary of Ni K-edge EXAFS fit parameters.
878
879

880 **References:**

881 Arai, Y., 2008. Spectroscopic Evidence for Ni(II) Surface Speciation at the Iron
882 Oxyhydroxides−Water Interface. Environmental Science & Technology, 42(4): 1151-1156.

883 Balistrieri, L.S., Borrok, D.M., Wanty, R.B., Ridley, W.I., 2008. Fractionation of Cu and Zn
884 isotopes during adsorption onto amorphous Fe(III) oxyhydroxide: Experimental mixing of
885 acid rock drainage and ambient river water. Geochimica Et Cosmochimica Acta, 72(2): 311-
886 328.

887 Barling, J., Anbar, A.D., 2004. Molybdenum isotope fractionation during adsorption by
888 manganese oxides. Earth and Planetary Science Letters, 217(3-4): 315-329.

889 Barrow, N.J., Brümmer, G.W., Fischer, L., 2012. Rate of desorption of eight heavy metals
890 from goethite and its implications for understanding the pathways for penetration. European
891 Journal of Soil Science, 63(3): 389-398.

892 Beard, B.L. et al., 2010. Iron isotope fractionation between aqueous ferrous iron and goethite.
893 Earth and Planetary Science Letters, 295(1-2): 241-250.

894 Bekker, A. et al., 2010. Iron Formation: The Sedimentary Product of a Complex Interplay
895 among Mantle, Tectonic, Oceanic, and Biospheric Processes. Economic Geology, 105(3):
896 467-508.

897 Bruemmer, G.W., Gerth, J., Tiller, K.G., 1988. Reaction kinetics of the adsorption and
898 desorption of nickel, zinc and cadmium by goethite. I. Adsorption and diffusion of metals.
899 Journal of Soil Science, 39(1): 37-52.

900 Bruland, K.W., 1980. Oceanographic distributions of Cadmium, Zinc, Nickel, and Copper in
901 the North Pacific. Earth and Planetary Science Letters, 47(2): 176-198.

902 Brümmer, G.W., Barrow, N.J., Fischer, L., 2013. Effect of porosity of goethite on the sorption
903 of six heavy metal ions. European Journal of Soil Science, 64(6): 805-813.

904 Butt, C.R.M., Cluzel, D., 2013. Nickel Laterite Ore Deposits: Weathered Serpentinites.
905 Elements, 9(2): 123-128.

906 Callender, E., 2014. Heavy Metals in the Environment – Historical Trends A2 - Holland,
907 Heinrich D. In: Turekian, K.K. (Ed.), Treatise on Geochemistry (Second Edition). Elsevier,
908 Oxford, pp. 59-89.

909 Cameron, V., Vance, D., 2014. Heavy nickel isotope compositions in rivers and the oceans.
910 Geochimica Et Cosmochimica Acta, 128(0): 195-211.

911 Cameron, V., Vance, D., Archer, C., House, C.H., 2009. A biomarker based on the stable
912 isotopes of nickel. Proceedings of the National Academy of Sciences of the United States of
913 America, 106(27): 10944-10948.

914 Carvalho-E-Silva, M.L. et al., 2003. Incorporation of Ni into natural goethite: An
915 investigation by X-ray absorption spectroscopy. American Mineralogist, 88(5): 876-882.

916 Cismasu, A.C., Levard, C., Michel, F.M., Brown Jr, G.E., 2013. Properties of impurity-
917 bearing ferrihydrite II: Insights into the surface structure and composition of pure, Al- and Si-
918 bearing ferrihydrite from Zn(II) sorption experiments and Zn K-edge X-ray absorption
919 spectroscopy. Geochimica et Cosmochimica Acta, 119(0): 46-60.

920 Cornell, R.M., Giovanoli, R., Schneider, W., 1992. The effect of Nickel on the conversion of
921 amorphous iron(III) hydroxide into more crystalline iron-oxides in alkaline media. Journal of
922 Chemical Technology and Biotechnology, 53(1): 73-79.

923 Cornell, R.M., Schwertmann, U., 1979. Influence of organic-anions on the crystallization of
924 ferrihydrite. Clays and Clay Minerals, 27(6): 402-410.

925 Cornell, R.M., Schwertmann, U., 2003. The Iron Oxides: Structure, Properties, Reactions,
926 Occurrences and Uses. Wiley, New York, 603 pp.

927 Davis, J.A., Kent, D.B., 1990. Surface complexation modeling in aqueous geochemistry.
928 Mineral-Water Interface Geochemistry, 23.

929 Dublet, G. et al., 2012. Ni speciation in a New Caledonian lateritic regolith: A quantitative X-
930 ray absorption spectroscopy investigation. Geochimica et Cosmochimica Acta, 95(0): 119-
931 133.

932 Dublet, G. et al., 2014. XAS evidence for Ni sequestration by siderite in a lateritic Ni-deposit
933 from New Caledonia, American Mineralogist, pp. 225.

934 Dzombak, D.A., Morel, F.M.M., 1990. Surface complexation modeling : hydrous ferric oxide.
935 Wiley, New York.

936 Eickhoff, M. et al., 2014. Nickel partitioning in biogenic and abiogenic ferrihydrite: The
937 influence of silica and implications for ancient environments. Geochimica et Cosmochimica
938 Acta, 140(0): 65-79.

939 Ellis, A.S., Johnson, T.M., Bullen, T.D., 2004. Using Chromium Stable Isotope Ratios To
940 Quantify Cr(VI) Reduction: Lack of Sorption Effects. Environmental Science & Technology,
941 38(13): 3604-3607.

942 Essington, M.E., 2003. Surface chemistry and adsorption reactions, Soil and water chemistry.
943 CRC Press LLC, Boca Raton, FL.

944 Fischer, L., Brümmer, G.W., Barrow, N.J., 2007. Observations and modelling of the reactions
945 of 10 metals with goethite: adsorption and diffusion processes. European journal of soil
946 science, 58(6): 1304-1315.

947 Frierdich, A.J., Beard, B.L., Reddy, T.R., Scherer, M.M., Johnson, C.M., 2014. Iron isotope
948 fractionation between aqueous Fe(II) and goethite revisited: New insights based on a multi-
949 direction approach to equilibrium and isotopic exchange rate modification. Geochimica et
950 Cosmochimica Acta, 139(0): 383-398.

951 Frierdich, A.J., Luo, Y., Catalano, J.G., 2011. Trace element cycling through iron oxide
952 minerals during redox-driven dynamic recrystallization. Geology, 39(11): 1083-1086.

Gaillardet, J., Viers, J., Dupré, B., 2014. Trace Elements in River Waters. In: Turekian, H.D.H.K. (Ed.), Treatise on Geochemistry (Second Edition). Elsevier, Oxford, pp. 195-235.

Gall, L. et al., 2013. Nickel isotopic compositions of ferromanganese crusts and the constancy of deep ocean inputs and continental weathering effects over the Cenozoic. Earth and Planetary Science Letters, 375(0): 148-155.

Goldberg, T., Archer, C., Vance, D., Poulton, S.W., 2009. Mo isotope fractionation during adsorption to Fe (oxyhydr)oxides. Geochimica et Cosmochimica Acta, 73(21): 6502-6516.

Gueguen, B., Rouxel, O., Ponzevera, E., Bekker, A., Fouquet, Y., 2013. Nickel Isotope Variations in Terrestrial Silicate Rocks and Geological Reference Materials Measured by MC-ICP-MS. Geostandards and Geoanalytical Research, 37(3): 297-317.

Gueguen, B. et al., 2016. Comparative geochemistry of four ferromanganese crusts from the Pacific Ocean and significance for the use of Ni isotopes as paleoceanographic tracers. Geochimica et Cosmochimica Acta.

Hayes, K.F., Redden, G., Ela, W., Leckie, J.O., 1991. Surface complexation models: An evaluation of model parameter estimation using FITEQL and oxide mineral titration data. Journal of Colloid and Interface Science, 142(2): 448-469.

Hofmann, A. et al., 2014. Comparing orthomagmatic and hydrothermal mineralization models for komatiite-hosted nickel deposits in Zimbabwe using multiple-sulfur, iron, and nickel isotope data. Mineralium Deposita, 49(1): 75-100.

Icopini, G.A., Anbar, A.D., Ruebush, S.S., Tien, M., Brantley, S.L., 2004. Iron isotope fractionation during microbial reduction of iron: The importance of adsorption. Geology, 32(3): 205-208.

Jiskra, M., Wiederhold, J.G., Bourdon, B., Kretzschmar, R., 2012. Solution Speciation Controls Mercury Isotope Fractionation of Hg(II) Sorption to Goethite. Environmental Science & Technology, 46(12): 6654-6662.

Juillot, F. et al., 2008. Zn isotopic fractionation caused by sorption on goethite and 2-Lines ferrihydrite. Geochimica Et Cosmochimica Acta, 72(19): 4886-4900.

Kashiwabara, T., Takahashi, Y., Tanimizu, M., 2009. A XAFS study on the mechanism of isotopic fractionation of molybdenum during its adsorption on ferromanganese oxides. GEOCHEMICAL JOURNAL, 43(6): e31-e36.

Kelly, S.D., Hesterberg, D., Ravel, B., 2008. Analysis of Soils and Minerals Using X-ray Absorption Spectroscopy, Methods of Soil Analysis. Soil Science Society of America, Madison, WI.

Konhauser, K.O. et al., 2009. Oceanic nickel depletion and a methanogen famine before the Great Oxidation Event. Nature, 458(7239): 750-754.

Konhauser, K.O. et al., 2015. The Archean Nickel Famine Revisited. Astrobiology, 15(10): 804-815.

Koschinsky, A., Halbach, P., 1995. Sequential leaching of marine ferromanganese precipitates: Genetic implications. Geochimica et Cosmochimica Acta, 59(24): 5113-5132.

Krishnaswami, S., 1976. Authigenic transition elements in Pacific pelagic clays. Geochimica Et Cosmochimica Acta, 40(4): 425-434.

Leinen, M., 1987. The origin of paleochemical signatures in North Pacific pelagic clays: Partitioning experiments. Geochimica et Cosmochimica Acta, 51(2): 305-319.

Li, X.F., Liu, Y., 2010. First-principles study of Ge isotope fractionation during adsorption onto Fe(III)-oxyhydroxide surfaces. Chemical Geology, 278(1–2): 15-22.

Manceau, A., Calas, G., 1985. Heterogeneous distribution of nickel in hydrous silicates from New Caledonia ore deposits. American Mineralogist, 70(5-6): 549-558.

Manceau, A., Drits, V.A., 1993. Local structure of ferrihydrite and feroxyhite by EXAFS spectroscopy. Clay Minerals, 28(2): 165-184.

Manceau, A., Gates, W.P., 1997. Surface structural model for ferrihydrite. Clays and Clay Minerals, 45(3): 448-460.

Manceau, A., Llorca, S., Calas, G., 1987. Crystal chemistry of cobalt and nickel in lithiophorite and asbolane from New Caledonia. Geochimica Et Cosmochimica Acta, 51(1): 105-113.

Manceau, A. et al., 2000. Crystal chemistry of trace elements in natural and synthetic goethite. Geochimica et Cosmochimica Acta, 64(21): 3643-3661.

Manceau, A. et al., 2002. Deciphering Ni sequestration in soil ferromanganese nodules by combining X-ray fluorescence, absorption, and diffraction at micrometer scales of resolution. American Mineralogist, 87(10): 1494-1499.

Martin, J.M., Meybeck, M., 1979. Elemental mass-balance of material carried by major world rivers. Marine Chemistry, 7(3): 173-206.

Mikutta, C. et al., 2009. Iron isotope fractionation and atom exchange during sorption of ferrous iron to mineral surfaces. Geochimica et Cosmochimica Acta, 73(7): 1795-1812.

Mitchell, K., Couture, R.-M., Johnson, T.M., Mason, P.R.D., Van Cappellen, P., 2013. Selenium sorption and isotope fractionation: Iron(III) oxides versus iron(II) sulfides. Chemical Geology, 342: 21-28.

Morel, F.M.M., Price, N.M., 2003. The Biogeochemical Cycles of Trace Metals in the Oceans. Science, 300(5621): 944.

Mouvet, C., Bourg, A.C.M., 1983. Speciation (including adsorbed species) of copper, lead, nickel and zinc in the Meuse River: Observed results compared to values calculated with a chemical equilibrium computer program. Water Research, 17(6): 641-649.

Navrotsky, A., Mazeina, L., Majzlan, J., 2008. Size-Driven Structural and Thermodynamic Complexity in Iron Oxides. Science, 319(5870): 1635-1638.

1026 Peacock, C.L., Sherman, D.M., 2007a. Sorption of Ni by birnessite: Equilibrium controls on
1027 Ni in seawater. Chemical Geology, 238(1-2): 94-106.

1028 Peacock, C.L., Sherman, D.M., 2007b. Crystal-chemistry of Ni in marine ferromanganese
1029 crusts and nodules. American Mineralogist, 92(7): 1087-1092.

1030 Peña, J., Kwon, K.D., Refson, K., Bargar, J.R., Sposito, G., 2010. Mechanisms of nickel
1031 sorption by a bacteriogenic birnessite. Geochimica et Cosmochimica Acta, 74(11): 3076-
1032 3089.

1033 Pokrovsky, O.S., Galy, A., Schott, J., Pokrovski, G.S., Mantoura, S., 2014. Germanium
1034 isotope fractionation during Ge adsorption on goethite and its coprecipitation with Fe
1035 oxy(hydr)oxides. Geochimica et Cosmochimica Acta, 131(0): 138-149.

1036 Pokrovsky, O.S., Viers, J., Emnova, E.E., Kompantseva, E.I., Freydier, R., 2008. Copper
1037 isotope fractionation during its interaction with soil and aquatic microorganisms and metal
1038 oxy(hydr)oxides: Possible structural control. Geochimica et Cosmochimica Acta, 72(7): 1742-
1039 1757.

1040 Pokrovsky, O.S., Viers, J., Freydier, R., 2005. Zinc stable isotope fractionation during its
1041 adsorption on oxides and hydroxides. Journal of Colloid and Interface Science, 291(1): 192-
1042 200.

1043 Porter, S.J., Selby, D., Cameron, V., 2014. Characterising the nickel isotopic composition of
1044 organic-rich marine sediments. Chemical Geology, 387(0): 12-21.

1045 Price, N.M., Morel, F.M.M., 1991. Colimitation of phytoplankton growth by Nickel and
1046 Nitrogen. Limnology and Oceanography, 36(6): 1071-1077.

1047 Quantin, C., Ettler, V., Garnier, J., Šebek, O., 2008. Sources and extractibility of chromium
1048 and nickel in soil profiles developed on Czech serpentinites. Comptes Rendus Geoscience,
1049 340(12): 872-882.

1050 Ratié, G. et al., 2015. Nickel isotope fractionation during tropical weathering of ultramafic
1051 rocks. Chemical Geology, 402(0): 68-76.

1052 Ravel, B., Newville, M., 2005. ATHENA, ARTEMIS, HEPHAESTUS: data analysis for X-
1053 ray absorption spectroscopy using IFEFFIT. Journal of Synchrotron Radiation, 12: 537-541.

1054 Rehkämper, M. et al., 2002. Thallium isotope variations in seawater and hydrogenetic,
1055 diagenetic, and hydrothermal ferromanganese deposits. Earth and Planetary Science Letters,
1056 197(1-2): 65-81.

1057 Schauble, E.A., 2004. Applying Stable Isotope Fractionation Theory to New Systems.
1058 Reviews in Mineralogy and Geochemistry, 55(1): 65-111.

1059 Schwertmann, U., Stanjek, H., Becher, H.-H., 2004. Long-term in vitro transformation of 2-
1060 line ferrihydrite to goethite/hematite at 4, 10, 15 and 25°C. Clay Minerals, 39(4): 433-438.

1061 Sclater, F.R., Boyle, E., Edmond, J.M., 1976. On the marine geochemistry of nickel. Earth
1062 and Planetary Science Letters, 31(1): 119-128.

1063 Siebert, C., Nagler, T.F., Kramers, J.D., 2001. Determination of molybdenum isotope
1064 fractionation by double-spike multicollector inductively coupled plasma mass spectrometry.
1065 Geochemistry Geophysics Geosystems, 2: 1032.

1066 Siebert, C., Nagler, T.F., von Blanckenburg, F., Kramers, J.D., 2003. Molybdenum isotope
1067 records as a potential new proxy for paleoceanography. Earth and Planetary Science Letters,
1068 211(1-2): 159-171.

1069 Snodgrass, W.J., 1980. Distribution and behavior of nickel in the aquatic environment. New
1070 York, John Wiley & Sons, pp. 203-274.

1071 Soper, A.K., Neilson, G.W., Enderby, J.E., Howe, R.A., 1977. A neutron diffraction study of
1072 hydration effects in aqueous solutions. Journal of Physics C: Solid State Physics, 10(11):
1073 1793.

1074 Toner, B.M. et al., 2012. Mineralogy of iron microbial mats from loihi seamount. Frontiers in
1075 microbiology, 3.

1076 Turekian, K.K., 1977. The fate of metals in oceans. Geochimica Et Cosmochimica Acta,
1077 41(8): 1139-1144.

1078 Valeton, I., Biermann, M., Reche, R., Rosenberg, F., 1987. Genesis of nickel laterites and
1079 bauxites in greece during the jurassic and cretaceous, and their relation to ultrabasic parent
1080 rocks. Ore Geology Reviews, 2(4): 359-404.

1081 Vasyukova, E.V. et al., 2010. Trace elements in organic- and iron-rich surficial fluids of the
1082 boreal zone: Assessing colloidal forms via dialysis and ultrafiltration. Geochimica et
1083 Cosmochimica Acta, 74(2): 449-468.

1084 Villalobos, M., Trotz, M.A., Leckie, J.O., 2003. Variability in goethite surface site density:
1085 evidence from proton and carbonate sorption. Journal of Colloid and Interface Science,
1086 268(2): 273-287.

1087 Wasylenki, L.E., Howe, H.D., Spivak-Birndorf, L.J., Bish, D.L., 2015. Ni isotope
1088 fractionation during sorption to ferrihydrite: Implications for Ni in banded iron formations.
1089 Chemical Geology, 400(0): 56-64.

1090 Wasylenki, L.E., Swihart, J.W., Romaniello, S.J., 2014. Cadmium isotope fractionation
1091 during adsorption to Mn oxyhydroxide at low and high ionic strength. Geochimica et
1092 Cosmochimica Acta, 140(0): 212-226.

1093 Wasylenki, L.E. et al., 2011. The molecular mechanism of Mo isotope fractionation during
1094 adsorption to birnessite. Geochimica Et Cosmochimica Acta, 75(17): 5019-5031.

1095 Waychunas, G.A., Fuller, C.C., Davis, J.A., 2002. Surface complexation and precipitate
1096 geometry for aqueous Zn(II) sorption on ferrihydrite I: X-ray absorption extended fine
1097 structure spectroscopy analysis. Geochimica et Cosmochimica Acta, 66(7): 1119-1137.

1098 Webb, S.M., 2005. SIXpack: a graphical user interface for XAS analysis using IFEFFIT.
1099 Physica Scripta, 2005(T115): 1011.

1100 Wu, L., Percak-Dennett, E.M., Beard, B.L., Roden, E.E., Johnson, C.M., 2012. Stable iron
1101 isotope fractionation between aqueous Fe(II) and model Archean ocean Fe–Si coprecipitates
1102 and implications for iron isotope variations in the ancient rock record. Geochimica Et
1103 Cosmochimica Acta, 84(0): 14-28.

1104 Wu, L.L., Beard, B.L., Roden, E.E., Johnson, C.M., 2011. Stable Iron Isotope Fractionation
1105 Between Aqueous Fe(II) and Hydrous Ferric Oxide. Environmental Science & Technology,
1106 45(5): 1847-1852.

1107 Xu, Y., Axe, L., Yee, N., Dyer, J.A., 2006. Bidentate Complexation Modeling of Heavy
1108 Metal Adsorption and Competition on Goethite. Environmental Science & Technology, 40(7):
1109 2213-2218.

1110

1111

Table 1: Sample information, summary of experimental conditions, Ni loading to the mineral and Ni isotope composition (‰) of mineral phases and supernatant solutions for pH-dependent and variable Ni experiments.

Mineral	Sample name	Type of experiment	pH	$[Ni]_{aq}^{initial}$ (µmol/L)	Final loading to mineral (µmol Ni/g)[c]	Final loading to mineral (µmol Ni/m^2)[c]	% of Ni sorption[d]	$\delta^{60/58}Ni_{mineral}$	2se[e]	$\delta^{60/58}Ni_{aqueous}$	2se	$\Delta^{60/58}Ni_{min\text{-}aq}$[f]	2se[g]	Mass balance (‰)
2-line Ferrihydrite[a]	Fh-pH-01	pH dependent	5.0	170	1.99	0.02	1.2	-0.36	0.02	-0.32	0.03	-0.03	0.03	-0.32
2-line Ferrihydrite	Fh-pH-02	pH dependent	6.0	170	4.77	0.04	2.9	-0.47	0.02	-0.35	0.03	-0.12	0.04	-0.35
2-line Ferrihydrite	Fh-pH-03	pH dependent	7.0	170	38.21	0.32	23.4	-0.57	0.02	-0.30	0.03	-0.27	0.04	-0.36
2-line Ferrihydrite	Fh-pH-04	pH dependent	7.7	170	66.61	0.56	41.7	-0.52	0.02	-0.15	0.03	-0.37	0.04	-0.31
2-line Ferrihydrite	Fh-pH-05*	pH dependent	8.0	170	73.81	0.62	45.3	-0.55	0.02	-0.17	0.04	-0.38	0.05	-0.34
2-line Ferrihydrite	Fh-C-06	Varying initial [Ni]	7.7	17	12.97	0.11	78.1	-0.41	0.02	-0.02	0.04	-0.39	0.04	-0.33
2-line Ferrihydrite	Fh-C-07*	Varying initial [Ni]	7.7	85	38.64	0.32	46.8	-0.51	0.02	-0.18	0.04	-0.32	0.04	-0.34
2-line Ferrihydrite	Fh-C-08*	Varying initial [Ni]	7.7	170	41.31	0.35	24.8	-0.56	0.02	-0.22	0.04	-0.34	0.04	-0.30
2-line Ferrihydrite	Fh-C-09*	Varying initial [Ni]	7.7	341	131.24	1.10	39.2	-0.54	0.03	-0.13	0.04	-0.40	0.05	-0.29
2-line Ferrihydrite	Fh-C-10*	Varying initial [Ni]	7.7	426	203.14	1.71	49.8	-0.53	0.03	-0.28	0.04	-0.24	0.05	-0.40
Goethite[b]	Goe-pH-01	pH dependent	5.0	170	1.00	0.04	0.6	-1.00	0.03	-0.30	0.03	-0.70	0.04	-0.31
Goethite	Goe-pH-02	pH dependent	6.0	170	1.33	0.05	0.8	-1.13	0.03	-0.25	0.04	-0.88	0.05	-0.25
Goethite	Goe-pH-03	pH dependent	8.0	170	7.17	0.28	4.3	-1.19	0.03	-0.23	0.03	-0.96	0.05	-0.27
Goethite	Goe-C-04	Varying initial [Ni]	7.7	170	15.96	0.63	9.5	-1.08	0.02	-0.27	0.04	-0.80	0.04	-0.35
Goethite	Goe-C-05	Varying initial [Ni]	7.7	341	17.56	0.69	19.3	-1.15	0.02	-0.12	0.04	-1.03	0.04	-0.35
Goethite	Goe-C-06*	Varying initial [Ni]	7.7	426	33.86	1.33	7.9	-1.07	0.02	-0.29	0.03	-0.78	0.04	-0.35
Ni standard solution	-	-	-	-	-	-	-	-	-	-0.32	0.03	-	-	-
Ni standard solution	-	-	-	-	-	-	-	-	-	-0.34	0.03	-	-	-
Ni standard solution	-	-	-	-	-	-	-	-	-	-0.30	0.03	-	-	-
Ni standard solution	-	-	-	-	-	-	-	-	-	-0.35	0.06	-	-	-
Average Ni standard solution[h]	-	-	-	-	-	-	-	-	-	**-0.33**	**0.05 (2sd)**	-	-	-
Nod-A-1[i]	-	-	-	-	-	-	-	-	-	1.06	0.02	-	-	-
Nod-A-1[i]	-	-	-	-	-	-	-	-	-	1.01	0.03	-	-	-
Nod-A-1[i]	-	-	-	-	-	-	-	-	-	1.05	0.04	-	-	-
Nod-P-1[i]	-	-	-	-	-	-	-	-	-	0.30	0.03	-	-	-
Nod-P-1[i]	-	-	-	-	-	-	-	-	-	0.35	0.04	-	-	-
Nod-P-1[i]	-	-	-	-	-	-	-	-	-	0.34	0.03	-	-	-
Nod-P-1[i]	-	-	-	-	-	-	-	-	-	0.32	0.03	-	-	-

* Samples for which Ni K-edge EXAFS data were collected.

[a] 2-line ferrihydrite (0.014 mol Fe/g dry mineral)

[b] Goethite (0.015 mol Fe/g dry mineral)

[c] Final loading corresponds to the amount of Ni per gram or m^2 of mineral in the reactor. The amount of mineral added per reactor measured was ~ 0.15 g.

[d] Ni sorbed fractions (%) were determined by mass balance using measured amount of Ni in solution and adsorbed onto minerals.

[e] 2se corresponds to the two standard error of the mean determined on the 50 measurement cycles on the MC-ICP-MS for each sample (see text for explanation).

[f] The difference in isotopic composition between the mineral and the supernatant solution is expressed as $\Delta^{60/58}Ni_{min\text{-}aq} = \delta^{60/58}Ni_{mineral} - \delta^{60/58}Ni_{aqueous}$. This value corresponds to the fractionation factor during Ni adsorption on the mineral surface. A two-standard error was determined for this value by error propagation.

[g] '2se' corresponds to error propagation of the $\Delta^{60/58}Ni_{min/aq}$ values ($2se = \sqrt{((2se_{mineral})^2 + (2se_{aqueous})^2)}$).

[h] The initial Ni standard solution used for experiments was processed several times through chromatography columns. The two standard deviation (2sd, n=4) was calculated on these duplicates.

[i] Nod-A-1 and Nod-P-1 are duplicates of USGS geostandards measured for monitoring the reproducibility of the data.

Table 2: Sample information, summary of experimental conditions, Ni loading to the mineral and Ni isotope composition (‰) of mineral phases and supernatant solutions for the time-dependent experiments.

Mineral*	Sample name	Duration of experiment (hours)	pH	$[Ni]_{aq}^{initial}$ (µmol/L)	Final loading to mineral (µmol Ni/g)	Final loading to mineral (µmol Ni/m^2)	% of Ni sorption	$\delta^{60/58}Ni_{mineral}$	2se	$\delta^{60/58}Ni_{aqueous}$	2se	$\Delta^{60/58}Ni_{min-aq}$	2se	Mass balance (‰)
Goethite	Goe-T-07	18	7.7	170	41.0	1.6	22.3	-0.98	0.05	-0.21	0.06	-0.77	0.07	-0.38
Goethite	Goe-T-08	20	7.7	170	41.7	1.6	22.0	-0.96	0.05	-0.19	0.05	-0.77	0.07	-0.36
Goethite	Goe-T-09	22	7.7	170	42.2	1.7	22.6	-0.98	0.08	-0.26	0.03	-0.72	0.08	-0.42
Goethite	Goe-T-10	23	7.7	170	42.5	1.7	22.0	-0.98	0.04	-0.24	0.04	-0.74	0.05	-0.41
Goethite	Goe-T-11	18	7.7	426	65.3	2.6	17.2	-0.88	0.06	-0.25	0.04	-0.62	0.07	-0.36
Goethite	Goe-T-12	20	7.7	426	50.6	2.0	14.4	-0.99	0.06	-0.27	0.03	-0.73	0.07	-0.37
Goethite	Goe-T-13	22	7.7	426	56.7	2.2	15.6	-0.94	0.03	-0.29	0.06	-0.65	0.07	-0.39
Goethite	Goe-T-14	23	7.7	426	51.6	2.0	12.9	-0.97	0.05	-0.29	0.07	-0.68	0.08	-0.38
2-line Ferrihydrite	Fh-T-11	19	7.7	170	225.2	1.9	92.4	-0.36	0.04	0.00	0.05	-0.36	0.06	-0.33
2-line Ferrihydrite	Fh-T-12	20	7.7	170	224.5	1.9	92.9	-0.37	0.04	-0.02	0.03	-0.35	0.05	-0.35
2-line Ferrihydrite	Fh-T-13	22	7.7	170	223.5	1.9	93.2	-0.36	0.02	-0.01	0.04	-0.35	0.04	-0.34
2-line Ferrihydrite	Fh-T-14	23	7.7	170	322.7	2.7	95.0	-0.39	0.05	-0.05	0.03	-0.34	0.05	-0.38
2-line Ferrihydrite	Fh-T-15	19	7.7	426	444.4	3.7	91.5	-0.41	0.04	-0.03	0.05	-0.37	0.06	-0.37
2-line Ferrihydrite	Fh-T-16	20	7.7	426	443.1	3.7	91.5	-0.43	0.04	-0.05	0.05	-0.38	0.06	-0.40
2-line Ferrihydrite	Fh-T-17	22	7.7	426	392.9	3.3	85.7	-0.37	0.02	-0.05	0.04	-0.32	0.04	-0.33
2-line Ferrihydrite	Fh-T-18	23	7.7	426	443.1	3.7	91.3	-0.42	0.06	-0.06	0.01	-0.36	0.06	-0.39

*See Table 1 for footnotes.

Table 3: Summary of Ni EXAFS fit parameters.

Sample Name	Path	CN	R (Å)	σ^2 (Å^2)	ΔE_0 (eV)	χ	Red χ^2	R-factor
Fh-C-10	Ni-O	5.945 ± 0.644	2.050 ± 0.0078	0.0069 ± 0.0011	-5.273 ± 1.233	0.8088 ± 0.1304	23.39	0.0145
	Ni-Fe	1.618 ± 0.405	3.102 ± 0.0159	0.0079 ± 0.0017				
	Ni-Fe	0.574 ± 0.144	3.561 ± 0.0488	0.0079 ± 0.0017				
Fh-C-09	Ni-O	6.543 ± .0760	2.052 ± 0.0087	0.0082 ± 0.0013	-4.844 ± 1.275	0.7022 ± 0.1250	10.69	0.0166
	Ni-Fe	1.404 ± 0.351	3.096 ± 0.0187	0.0079 ± 0.0020				
	Ni-Fe	0.894 ± 0.224	3.596 ± 0.0347	0.0079 ± 0.0020				
Fh-C-08	Ni-O	6.507 ± 0.754	2.050 ± 0.0087	0.0084 ± 0.0013	-4.972 ± 1.275	0.8407 ± 0.1340	10.09	0.0162
	Ni-Fe	1.681 ± 0.420	3.102 ± 0.0161	0.0080 ± 0.0019				
	Ni-Fe	0.478 ± 0.120	3.593 ± 0.0618	0.0080 ± 0.0019				
Fh-C-07	Ni-O	6.441 ± 0.931	2.046 ± 0.0105	0.0068 ± 0.0015	-5.312 ± 1.666	0.7678 ± 0.1814	8.29	0.0261
	Ni-Fe	1.536 ± 0.384	3.112 ± 0.0239	0.0078 ± 0.0021				
	Ni-Fe	0.696 ± 0.174	3.524 ± 0.0583	0.0078 ± 0.0021				
Fh-pH-05	Ni-O	5.846 ± 0.767	2.046 ± 0.0092	0.0061 ± 0.0013	-5.446 ± 1.516	0.7287 ± 0.1532	11.31	0.0215
	Ni-Fe	1.457 ± 0.364	3.103 ± 0.0212	0.0076 ± 0.0021				
	Ni-Fe	0.814 ± 0.204	3.567 ± 0.0430	0.0076 ± 0.0021				
Goe-C-06	Ni-O	7.404 ± 0.861	2.045 ± 0.0092	0.0102 ± 0.0015	-6.092 ± 1.250	-	3.23	0.0100
	Ni-Fe	1.040 ± 0.445	3.070 ± 0.0277	0.0102 ± 0.0015				

CN: coordination number

R: interatomic distance

σ^2: Debye-Waller factor

ΔE_0: energy shift

Red χ^2: reduced chi squared statistic

S_0^2 : 0.96

K-range: 3-1

R-range: 1-4

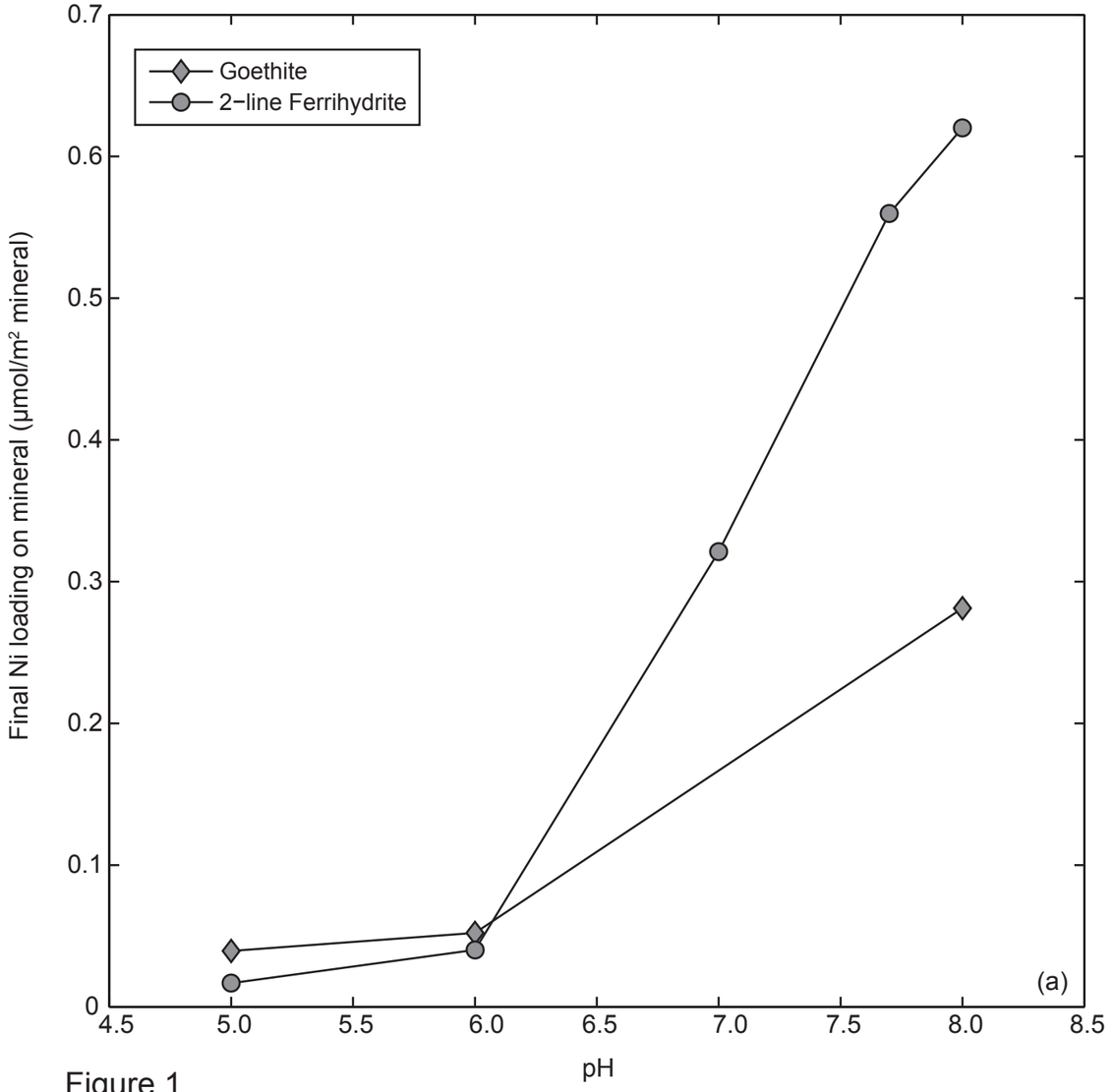
Goethite
2−line Ferrihydrite
Final Ni loading on mineral (μmol/m² mineral)
pH
(a)
0.7
0.6
0.5
0.4
0.3
0.2
0.1
0
4.5
5.0
5.5
6.0
6.5
7.0
7.5
8.0
8.5

Figure 1

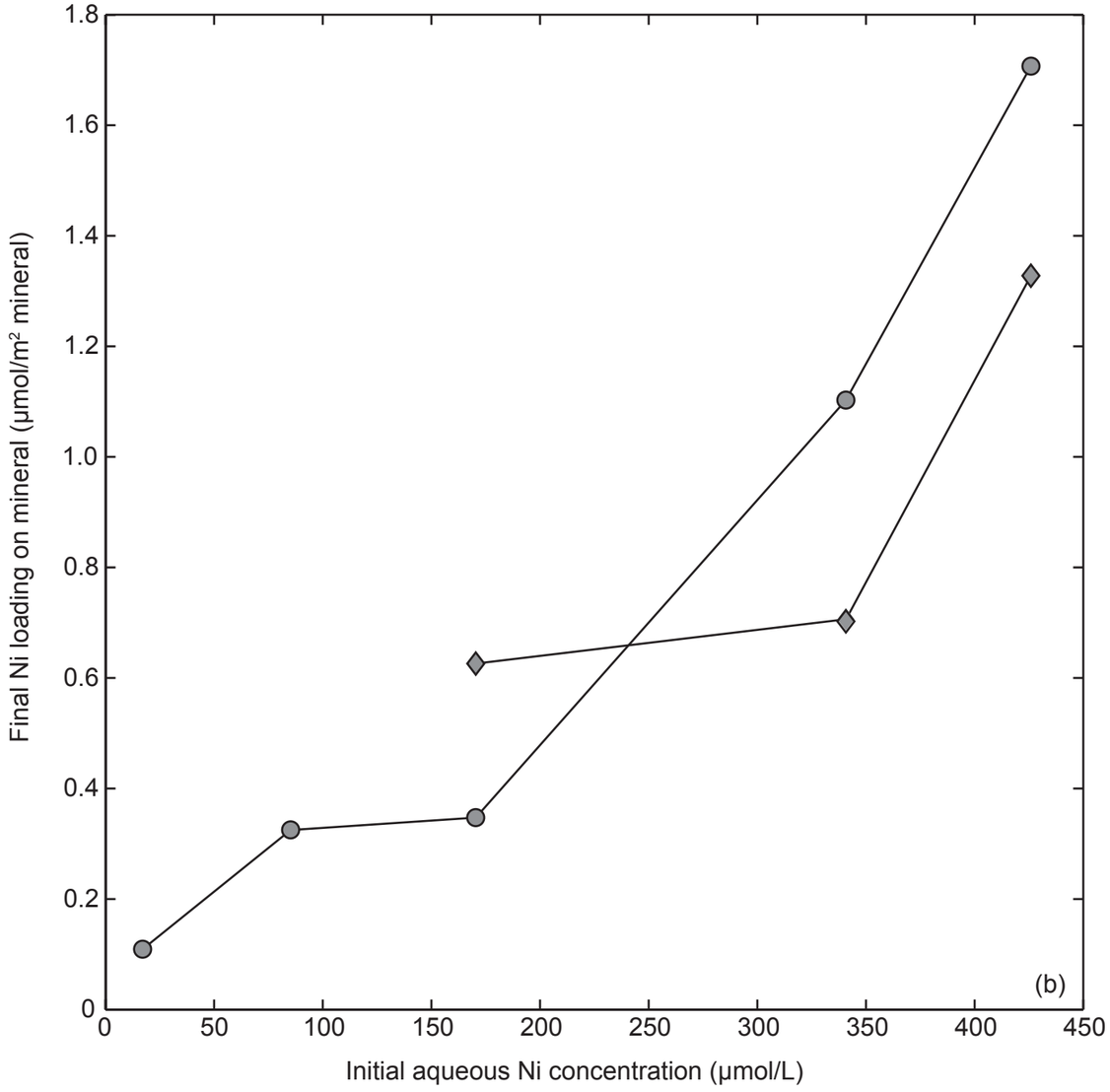
Final Ni loading on mineral (μmol/m² mineral)
Initial aqueous Ni concentration (μmol/L)
(b)
1.8
1.6
1.4
1.2
1.0
0.8
0.6
0.4
0.2
0
0
50
100
150
200
250
300
350
400
450

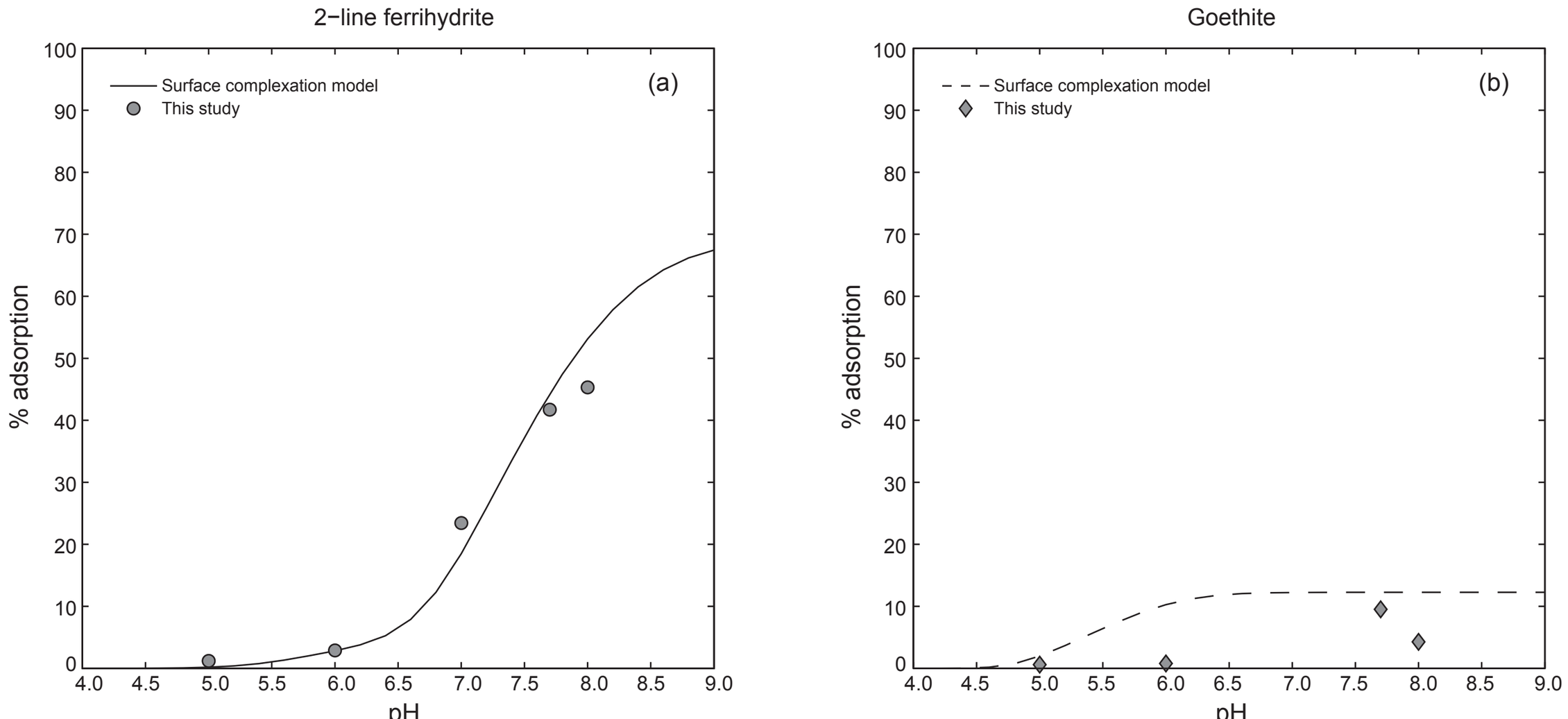
2−line ferrihydrite
Surface complexation model
This study
(a)
% adsorption
pH
Goethite
Surface complexation model
This study
(b)
% adsorption
pH

Figure 2

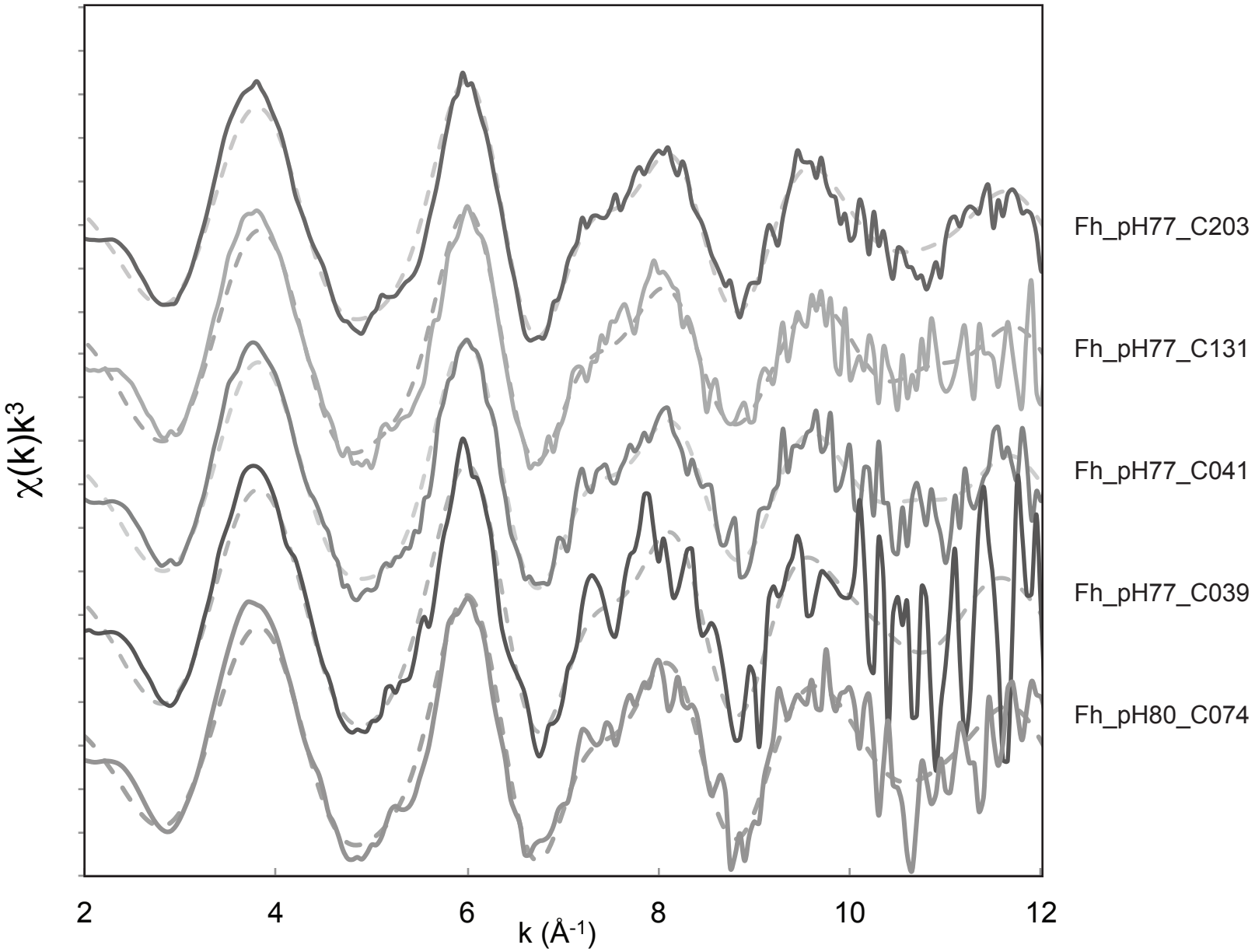
χ(k)k³
2
4
6
8
10
12
k (Å-1)
Fh_pH77_C203
Fh_pH77_C131
Fh_pH77_C041
Fh_pH77_C039
Fh_pH80_C074

Figure 3

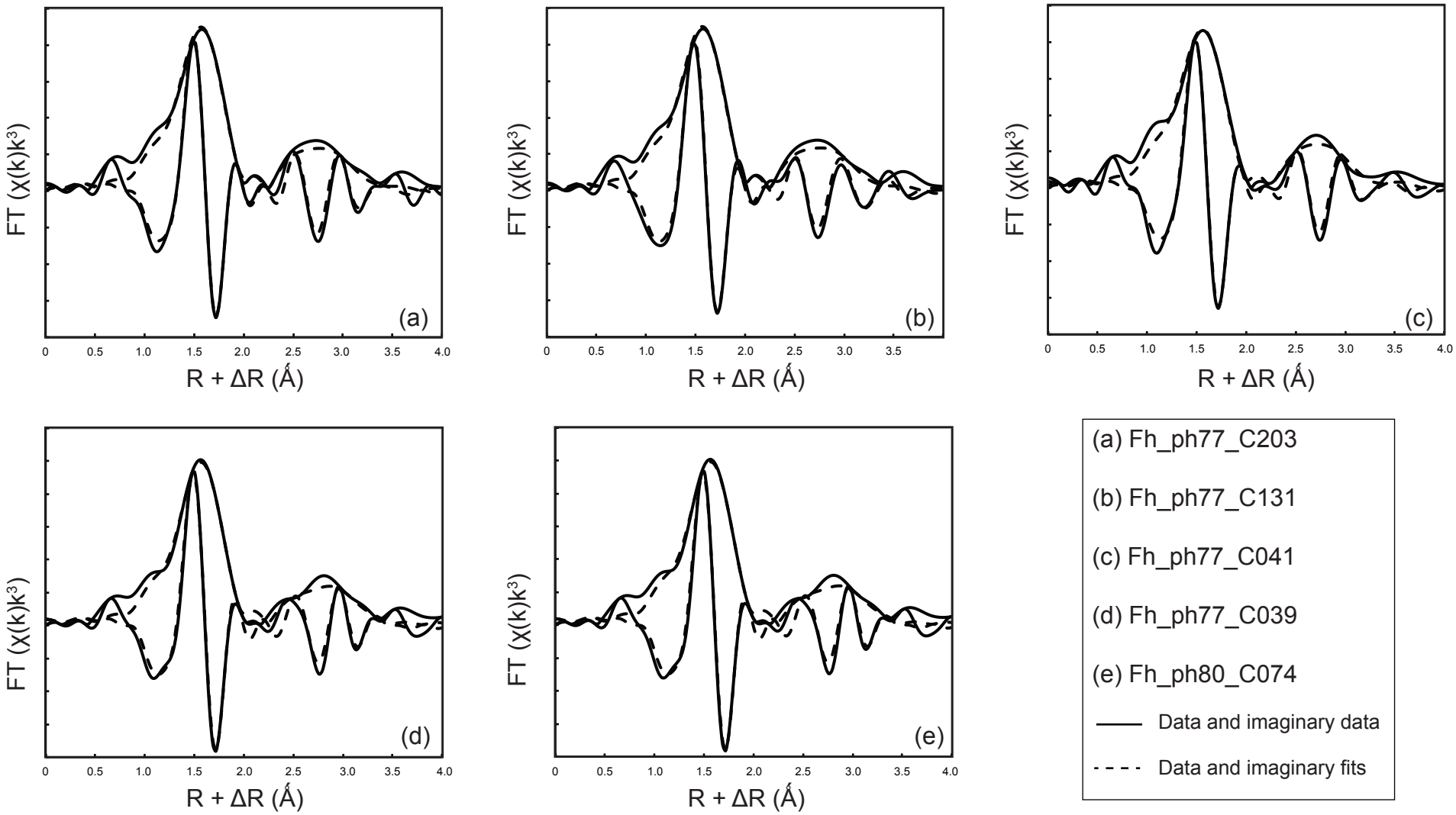
FT (χ(k)k³)
R + ΔR (Å)
(a)
(b)
(c)
(d)
(e)
0 0.5 1.0 1.5 2.0 2.5 3.0 3.5 4.0
(a) Fh_ph77_C203
(b) Fh_ph77_C131
(c) Fh_ph77_C041
(d) Fh_ph77_C039
(e) Fh_ph80_C074
Data and imaginary data
Data and imaginary fits

Figure 4

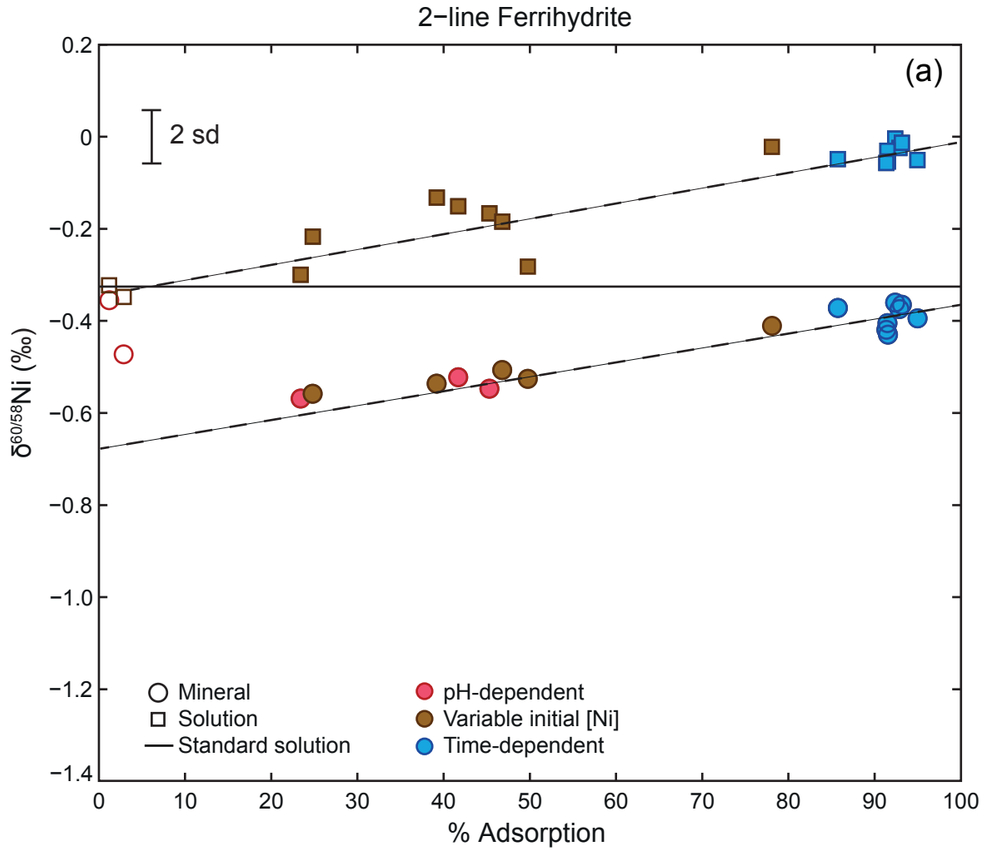
2−line Ferrihydrite
(a)
2 sd
δ60/58Ni (‰)
% Adsorption
Mineral
Solution
Standard solution
pH-dependent
Variable initial [Ni]
Time-dependent

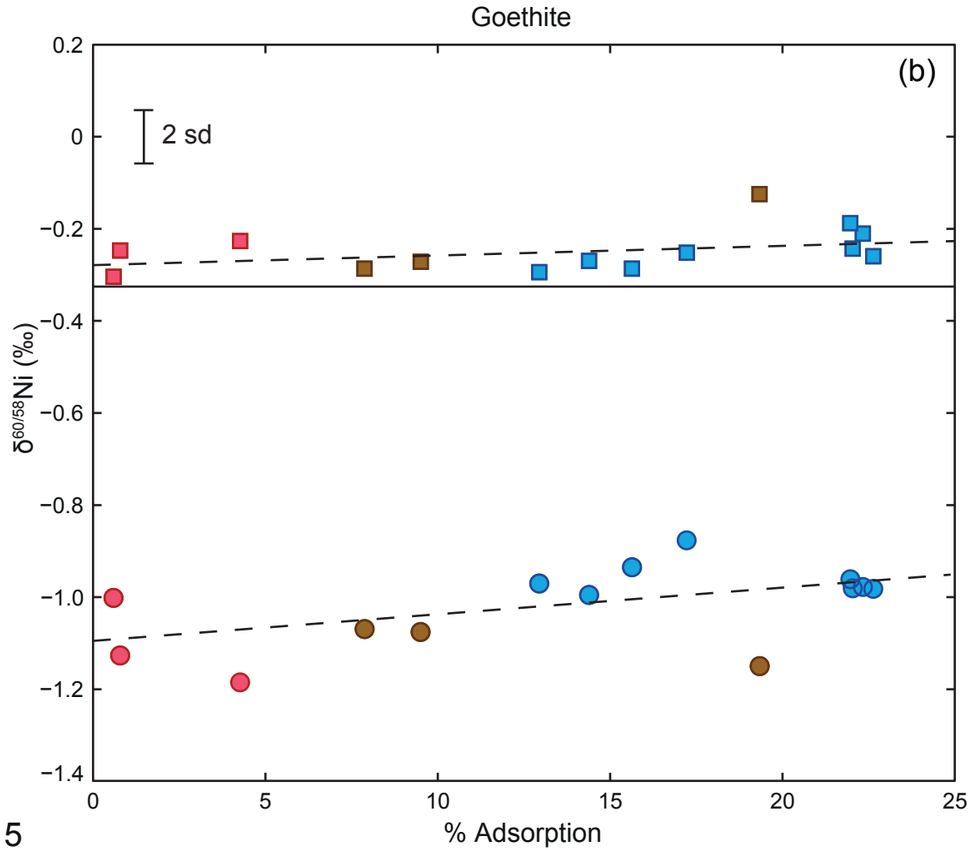
Goethite
(b)
2 sd
δ60/58Ni (‰)
% Adsorption

Figure 5

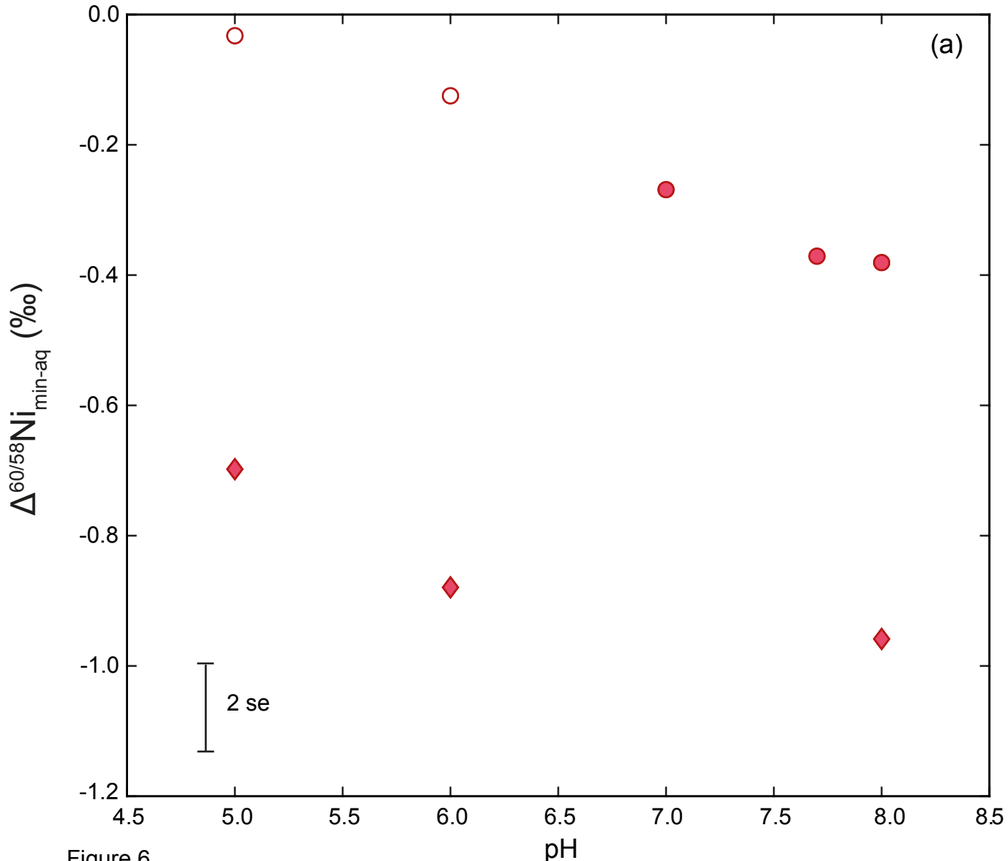
(a)
0.0
-0.2
-0.4
-0.6
-0.8
-1.0
-1.2
4.5
5.0
5.5
6.0
6.5
7.0
7.5
8.0
8.5
pH
$\Delta^{60/58}Ni_{min\text{-}aq}$ (‰)
2 se

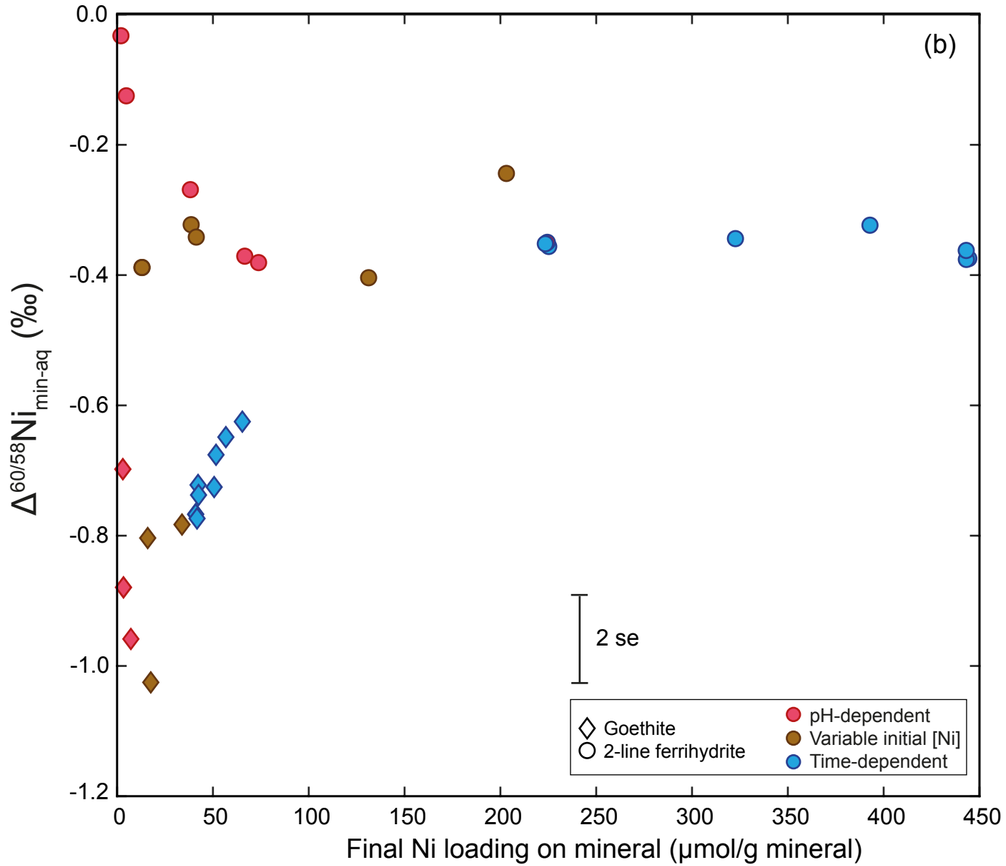
(b)
0.0
-0.2
-0.4
-0.6
-0.8
-1.0
-1.2
0
50
100
150
200
250
300
350
400
450
Final Ni loading on mineral (µmol/g mineral)
$\Delta^{60/58}Ni_{min\text{-}aq}$ (‰)
2 se
Goethite
2-line ferrihydrite
pH-dependent
Variable initial [Ni]
Time-dependent

Figure 6

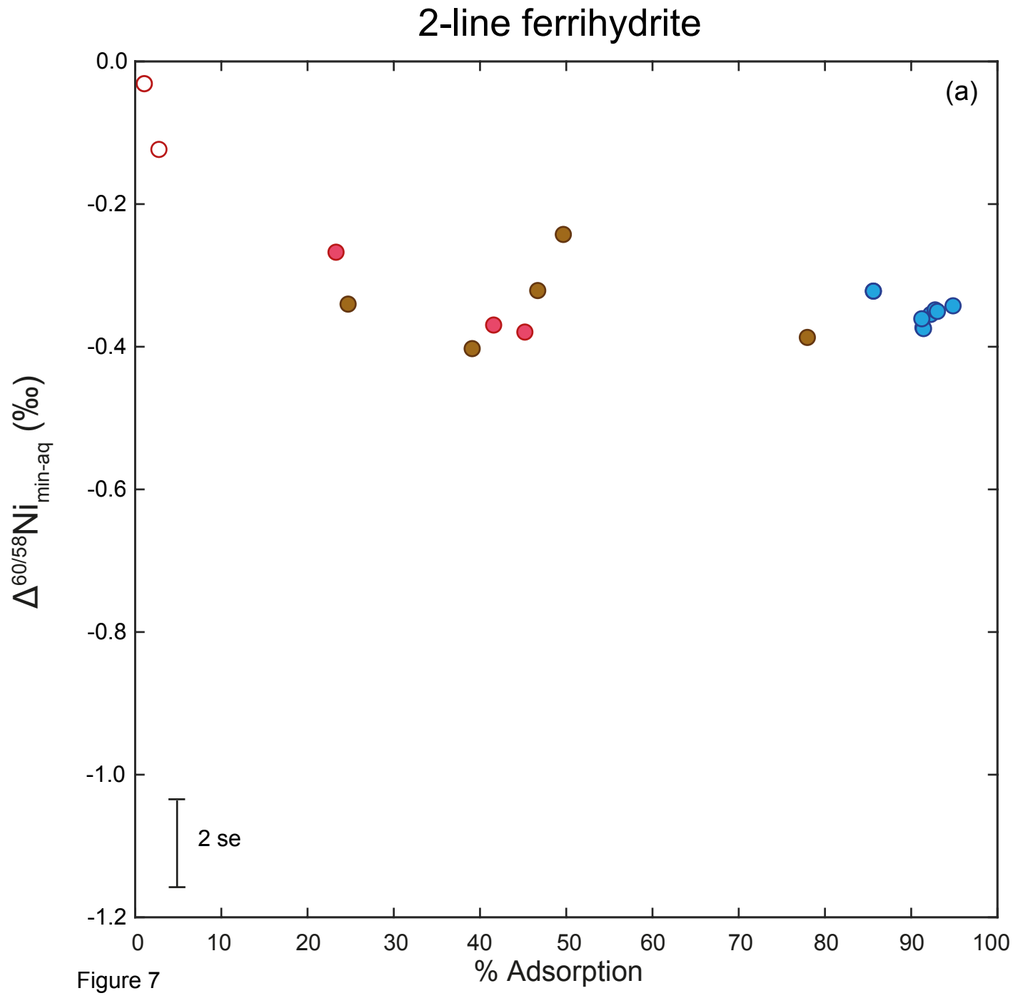
2-line ferrihydrite
(a)
0.0
-0.2
-0.4
-0.6
-0.8
-1.0
-1.2
$\Delta^{60/58}Ni_{min-aq}$ (‰)
2 se
0
10
20
30
40
50
60
70
80
90
100
% Adsorption

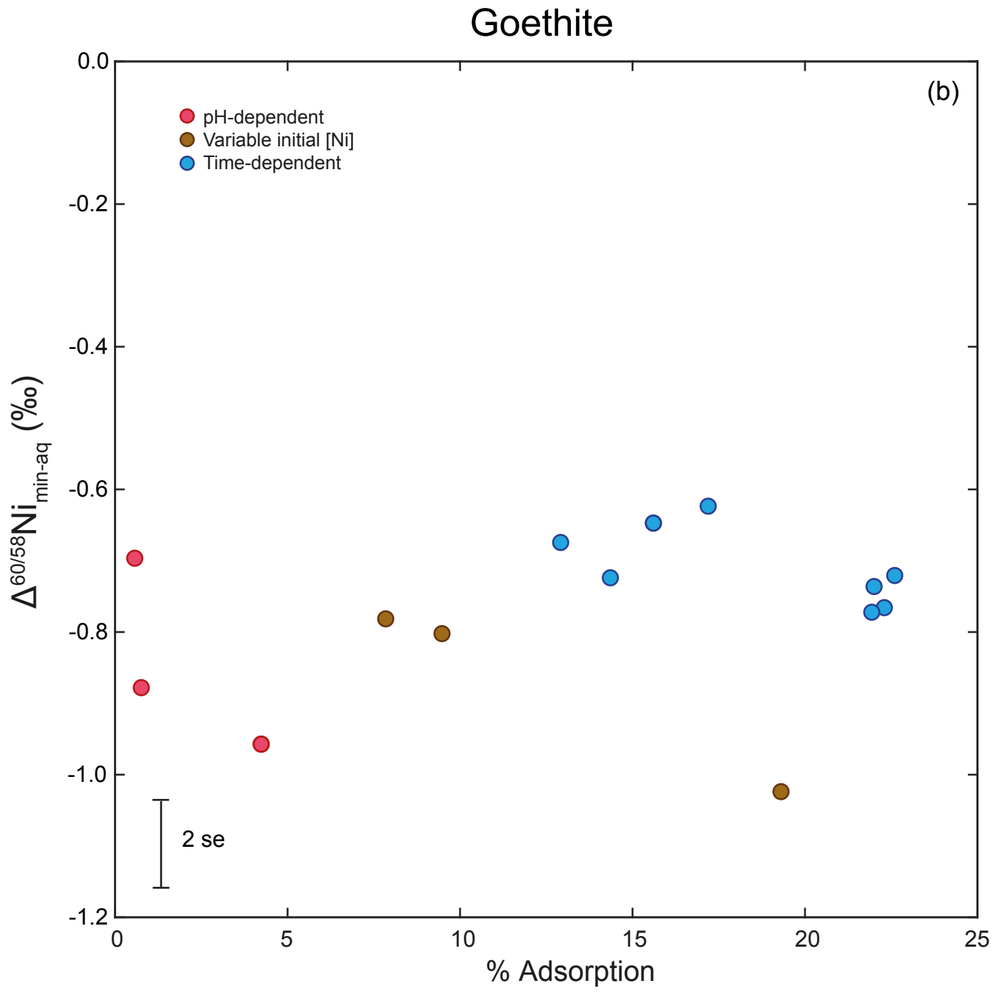
Goethite
(b)
pH-dependent
Variable initial [Ni]
Time-dependent
0.0
-0.2
-0.4
-0.6
-0.8
-1.0
-1.2
$\Delta^{60/58}Ni_{min-aq}$ (‰)
2 se
0
5
10
15
20
25
% Adsorption

Figure 7

Electronic Annex

Variable Ni isotope fractionation between Fe-oxyhydroxides and implications for the use of Ni isotopes as geochemical tracers

Bleuenn Gueguen[1,2*], Jeffry V. Sorensen[3], Stefan V. Lalonde[1], Jasquelin Peña[4], Brandy M. Toner[3], and Olivier Rouxel[2]

[1]Institut Universitaire Européen de la Mer, Laboratoire Domaines Océaniques UMR 6538, Université de Brest, 29280 Plouzané, France

[2]IFREMER, Centre de Brest, Unité Géosciences Marines, 29280 Plouzané, France

[3]Department of Soil, Water, and Climate, University of Minnesota, St. Paul, MN 55108, USA

[4]Institute of Earth Surface Dynamics, University of Lausanne, CH-1015 Lausanne, Switzerland

Submitted to Chemical Geology

*Corresponding author:

E-mail address: bleuenn.gueguen@univ-brest.fr

Current address: Institut Universitaire Européen de la Mer, CNRS UMS 3113, Université de Brest, 29280 Plouzané, France

Supplementary Figures :

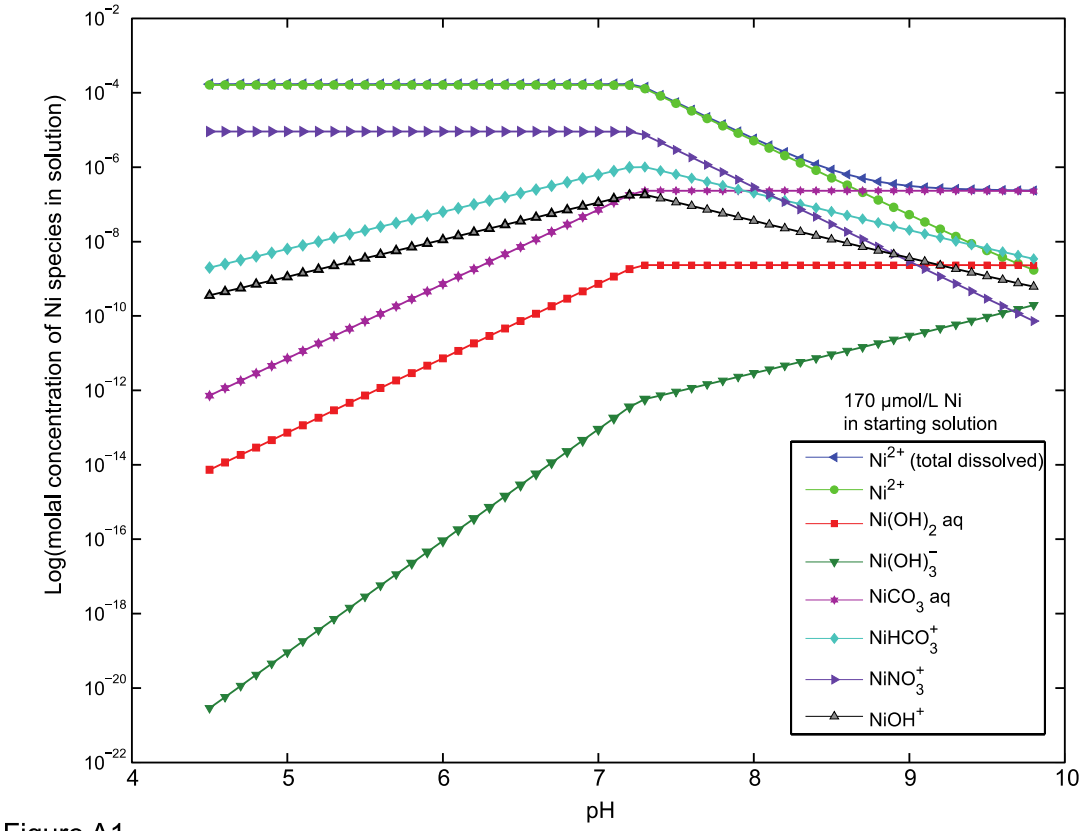

Figure A1

Figure A1: Nickel speciation modeling (logarithm of molal concentrations of different Ni species) versus pH of solution for 170 µmol/L of Ni in starting solution. The curves represent the different Ni species present in the system, i.e., Ni^{2+}, $Ni(OH)_{2aq}$, $Ni(OH)_3^-$, $NiCO_{3aq}$, $NiHCO_3^+$, $NiNO_3^+$, $NiOH^+$.

Figure A2: Cartoon showing Ni bonding environment according to a "Type 1" configuration or a "Type 2" configuration.

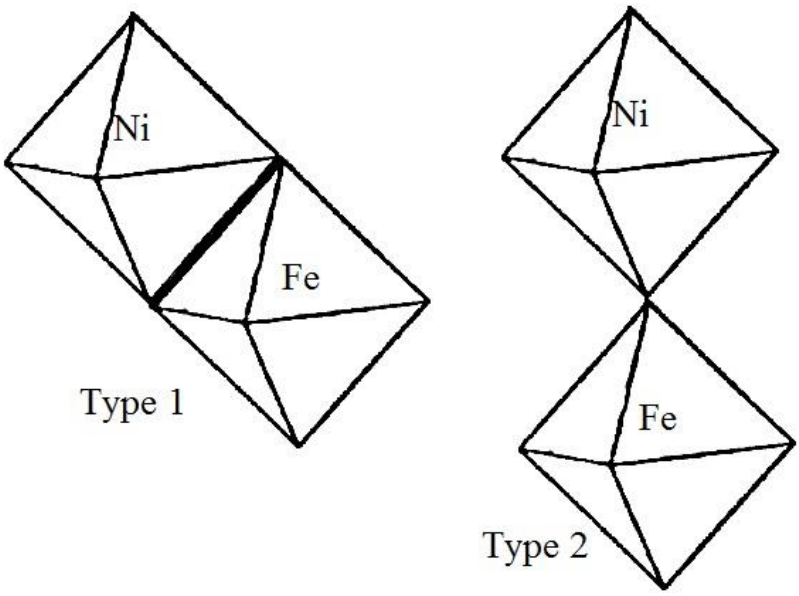

Figure A3: Nickel speciation versus pH of the solution for different initial Ni (aq), (a) 17 µmol Ni /L, (b) 85 µmol Ni /L, (c) 170 µmol Ni /L, (d) 341 µmol Ni /L, and (e) 426 µmol Ni /L.

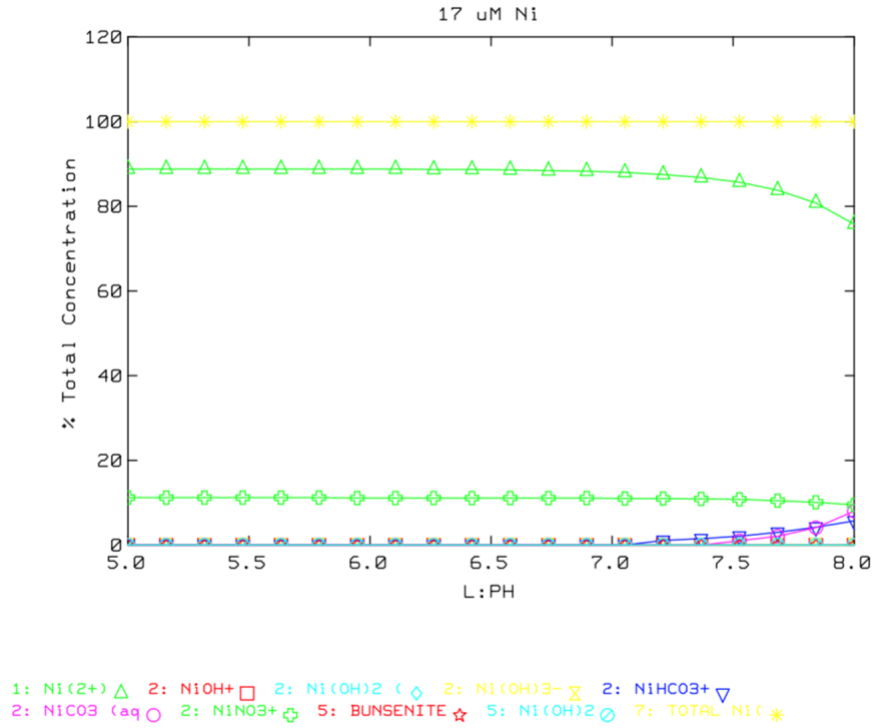

(a)

(b)

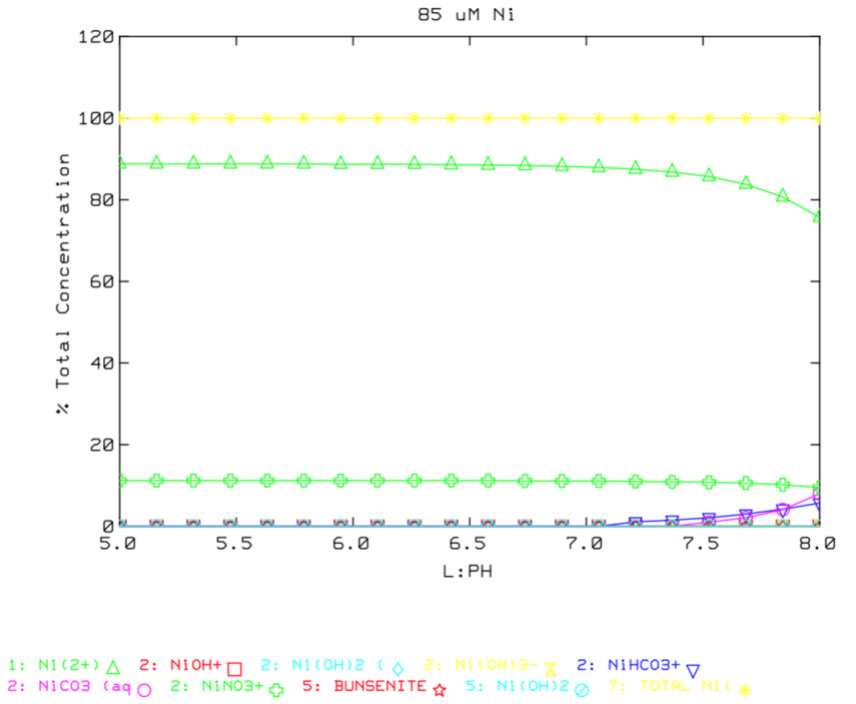
85 uM Ni
% Total Concentration
L:PH
1: Ni(2+)
2: NiOH+
2: Ni(OH)2 (
2: Ni(OH)3-
2: NiHCO3+
2: NiCO3 (aq
2: NiNO3+
5: BUNSENITE
5: Ni(OH)2
7: TOTAL Ni(

(c)

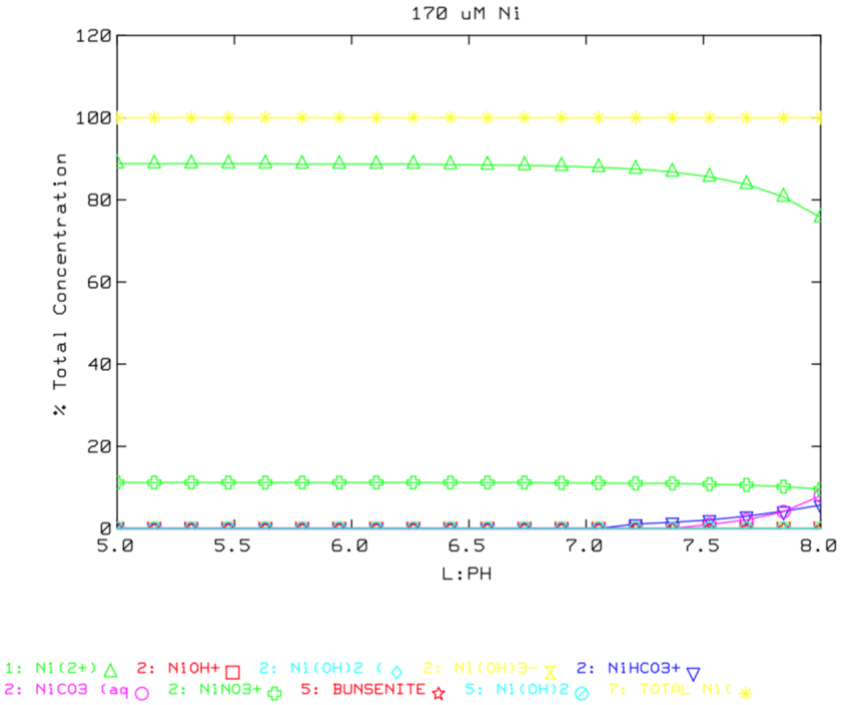
170 uM Ni
% Total Concentration
L:PH
1: Ni(2+)
2: NiOH+
2: Ni(OH)2 (
2: Ni(OH)3-
2: NiHCO3+
2: NiCO3 (aq
2: NiNO3+
5: BUNSENITE
5: Ni(OH)2
7: TOTAL Ni(

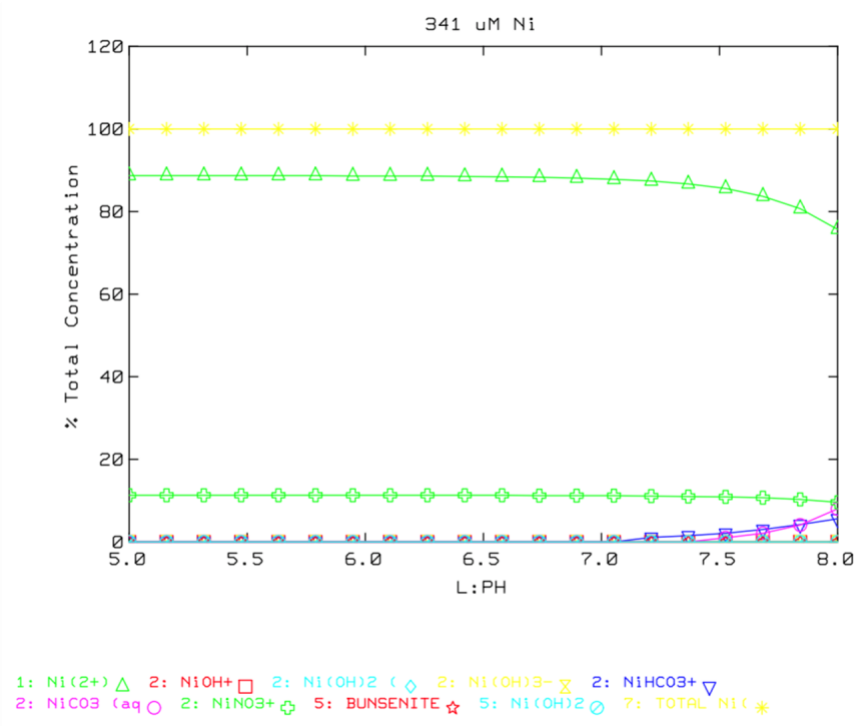
341 uM Ni
% Total Concentration
L:PH
120
100
80
60
40
20
0
5.0
5.5
6.0
6.5
7.0
7.5
8.0
1: Ni(2+)
2: NiOH+
2: Ni(OH)2 (
2: Ni(OH)3-
2: NiHCO3+
2: NiCO3 (aq
2: NiNO3+
5: BUNSENITE
5: Ni(OH)2
7: TOTAL Ni(

(d)

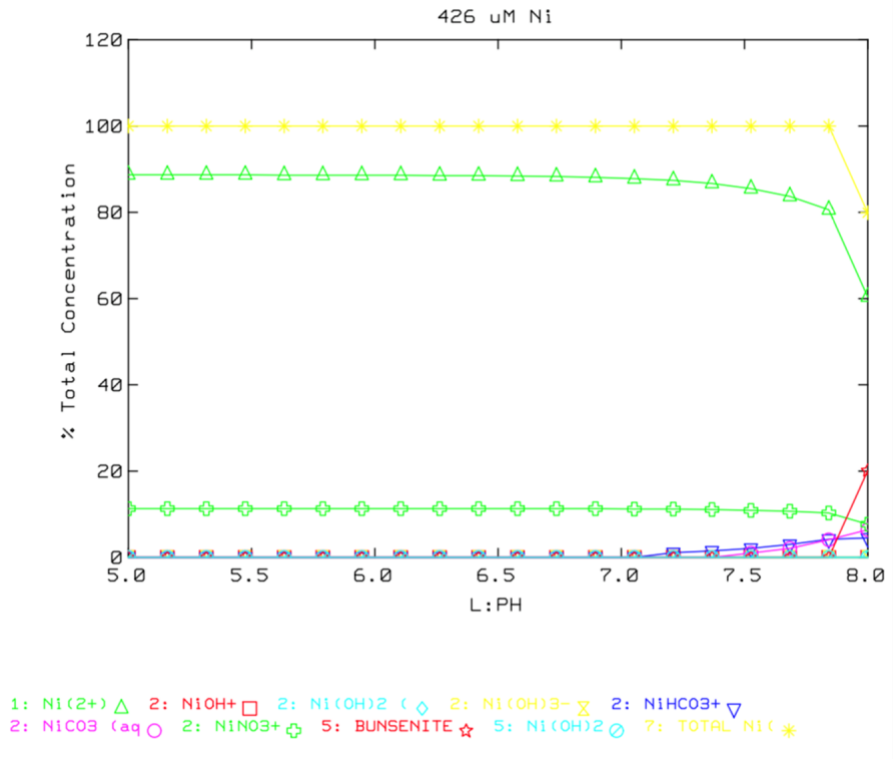
426 uM Ni
% Total Concentration
L:PH
120
100
80
60
40
20
0
5.0
5.5
6.0
6.5
7.0
7.5
8.0
1: Ni(2+)
2: NiOH+
2: Ni(OH)2 (
2: Ni(OH)3-
2: NiHCO3+
2: NiCO3 (aq
2: NiNO3+
5: BUNSENITE
5: Ni(OH)2
7: TOTAL Ni(

(e)

Supplementary Tables :

Table S1: Zeta potential measurement parameters.

Mineral type	Amount of mineral in solution	Conductance	Current	Applied Voltage	Zeta potential	Mobility	Relative Residual
2-line Ferrihydrite	1.44 g/L	344 µS	2.56 mA	7.54 V	-3.44 mV	-0.027	0.0093
Goethite	0.984 g/L	81 µS	0.712 mA	7.54 V	3.46 mV	0.27	0.0151

Table S2: Summary of EXAFS fit parameters for previous Ni-sorption and -incorporation experiments. Data for Zn are shown for comparison. Literature data is from (Manceau et al., 2000; Waychunas et al., 2002; Arai, 2008; Juillot et al., 2008; Dublet et al., 2012; Cismasu et al., 2013).

Sample type	Atom Pair	CN[1]	R (Å)[2]	σ^2 (Å^2)[3]	Reference
Ni-sorbed goethite	Ni-O	5.1	2.10	0.0049	Dublet et al. 2012
	Ni-Fe	1.5	3.00	0.0049	
	Ni-Fe	2.4	3.14	-	
Ni-sorbed goethite	Ni-O	5.7	2.06	0.0051	Arai, 2008
	Ni-Fe	1.2	3.03	0.0050	
	Ni-Fe	1.1	3.18	0.0050	
	Ni-Fe	1.7	4.06	0.0080	
Zn-sorbed goethite	Zn-O	4.6	2.06	0.0081	Juillot et al. 2008
	Zn-Fe	0.9	3.07	0.0081	
	Zn-Fe	0.8	3.26	-	
Zn-sorbed ferrihydrite	Zn-O	3.6	1.98	0.006	Cismasu et al. 2013
	Zn-Fe	0.9	3.21	0.011	
	Zn-Fe	1.9	3.44	0.01	
Zn-sorbed ferrihydrite	Zn-O	5.05	1.96	0.007	Waychunas et al. 2002
	Zn-Fe	1.93	3.43	0.012	
Zn-sorbed ferrihydrite	Zn-O	3.2	1.96	0.0049	Juillot et al. 2008
	Zn-Fe	1	3.47	0.01	
Ni-sorbed ferrihydrite	Ni-O	5.9	2.05	0.0054	Arai, 2008
	Ni-Fe	1.0	3.08	0.0050	
	Ni-Fe	1.8	3.21	0.0050	
	Ni-Fe	1.0	4.03	0.0080	
Ni-sorbed ferrihydrite	Ni-O	5.7	2.06	0.0060	Arai, 2008
	Ni-Fe	1.4	3.05	0.0050	
	Ni-Fe	1.9	3.21	0.0050	
	Ni-Fe	1.1	4.05	0.0080	
Ni-sorbed ferrihydrite	Ni-O	5.8	2.06	0.006	Arai 2008
	Ni-Fe	1.5	3.06	0.0050	
	Ni-Fe	1.3	3.19	0.0050	
	Ni-Fe	0.9	4.07	0.0080	
Ni-bearing goethite	Ni-O	5.3	2.07	0.0036	Manceau et al. 2000
	Ni-Fe	2.1	3.00	0.0064	
	Ni-Fe	1.4	3.18	0.0064	
	Ni-Fe	2.5	3.62	0.0064	
Ni-bearing goethite	Ni-O	5.7	2.05	0.0049	Dublet et al. 2012
	Ni-Fe	2.0	2.98	0.0049	
	Ni-Fe	2.0	3.16	-	
	Ni-Fe	1.2	3.57	-	

[1,2,3] See Table 2 and main text.

References :

Arai, Y., 2008. Spectroscopic Evidence for Ni(II) Surface Speciation at the Iron Oxyhydroxides−Water Interface. Environmental Science & Technology, 42(4): 1151-1156.

Cismasu, A.C., Levard, C., Michel, F.M., Brown Jr, G.E., 2013. Properties of impurity-bearing ferrihydrite II: Insights into the surface structure and composition of pure, Al- and Si-bearing ferrihydrite from Zn(II) sorption experiments and Zn K-edge X-ray absorption spectroscopy. Geochimica et Cosmochimica Acta, 119(0): 46-60.

Dublet, G. et al., 2012. Ni speciation in a New Caledonian lateritic regolith: A quantitative X-ray absorption spectroscopy investigation. Geochimica et Cosmochimica Acta, 95(0): 119-133.

Juillot, F. et al., 2008. Zn isotopic fractionation caused by sorption on goethite and 2-Lines ferrihydrite. Geochimica Et Cosmochimica Acta, 72(19): 4886-4900.

Manceau, A. et al., 2000. Crystal chemistry of trace elements in natural and synthetic goethite. Geochimica et Cosmochimica Acta, 64(21): 3643-3661.

Waychunas, G.A., Fuller, C.C., Davis, J.A., 2002. Surface complexation and precipitate geometry for aqueous Zn(II) sorption on ferrihydrite I: X-ray absorption extended fine structure spectroscopy analysis. Geochimica et Cosmochimica Acta, 66(7): 1119-1137.